Ocean Circulation and Marine Terminating Glaciers of the Greenland Ice Sheet

by

Laura C. Gillard

A thesis submitted in partial fulfillment of the requirements for the degree of

Master of Science

Department of Earth and Atmospheric Sciences
University of Alberta

Abstract

Higher latitudes have experienced a significant change in climate and physical processes within recent years. This study focuses on the Greenland Ice Sheet and surrounding ocean waters. It has been shown that relatively warm ocean waters may accelerate melt production of marine terminating glaciers. We explore and classify the pathways for the warmer Atlantic waters that reach the fjords along the coasts of Greenland. Additionally, given that the melt of these glaciers is accelerating, we look at the pathways of the low salinity melt waters from these coastal glaciers and where it is taken up in the surrounding basins. This analysis was carried out using an Arctic and North Hemisphere Atlantic (ANHA) configuration of the Nucleus for European Modelling of the Ocean (NEMO) ocean/sea-ice general circulation model run at both $\frac{1}{4}^o$ and $\frac{1}{12}^o$ resolution. Pathways were determined using the ARIANE Lagrangian float package using both forward and backward trajectories. Warm waters that reached the north and west coast of Greenland tended to be fed by the relatively warm and saline Irminger Current. The south east and the east Greenland coast tended to have warm waters advected to them through Nordic Seas.

Preface

This thesis is an original work done by Laura C. Gillard. No part of this thesis has been previously published. Chapter 3 of this thesis is being prepared to become a publication in Journal of Geophysical Research Letters, with authorship of Laura C. Gillard, Xianmin Hu and Paul G. Myers.

Acknowledgements

I would like to thank my supervisor, Professor Paul G. Myers for his guidance and encouragement throughout my time as his student.

Thank you to those in Paul Myers' Geophysical Fluid Dynamic Ocean Modelling Team for the lively discussions on our research, kind atmosphere and support. Sincere gratitude to Clark Pennelly for reading countless pages. I would like to thank Xianmin Hu for the contributions to work done in Chapter 3.

Thanks to Bruno Blanke and Nicolas Grima for the ARIANE tracking tool that I applied to the experiments. All model configurations used in this study was set up by Paul Myers' Geophysical Fluid Dynamic Ocean Modelling Team.
http://knossos.eas.ualberta.ca/xianmin/anha/index.html.

Contents

1 Background **1**

1.1 Introduction 1

1.2 Geography and Currents of Arctic 1

1.2.1 Warm Water Pulse 4

1.2.2 Canadian Arctic Archipelago 5

1.3 Baffin Bay 6

1.4 North Atlantic Subpolar Gyre 7

1.5 Enhanced Greenland Melt 10

1.6 Thesis Questions 11

1.7 Figures 15

2 Numerical Methods **17**

2.1 NEMO 17

2.2 Trajectory Calculation 24

2.2.1 Backward Trajectory Analysis 25

2.2.2 Forward Trajectory Analysis 25

2.3 Analysis 26

2.4 Figures and Tables 28

3 Ocean Circulation and Marine Terminating Glaciers of the Greenland Ice Sheet **32**

3.1 Abstract 32

3.2 Introduction 33

3.3 Methods 36
3.4 Results 41
3.4.1 Origin of Warm Water 41
3.4.2 Pathway of Fresh Meltwater 48
3.5 Discussion and Conclusions 51
3.6 Figures and Tables 55

4 Summary and Conclusions 70

List of Tables

2.1 Percentage Definition 28
2.2 Definition of relatively warm, saline waters that are found by the outlet regions 30
2.3 13 Outlet Region's of the Greenland Ice Sheet 30
2.4 Experiments using the ANHA-NEMO Configuration . 31

3.1 Depth Definition: Terminology used to classify the vertical water column of the model. 55

List of Figures

1.1 Ocean Circulation around Greenland and 13 outlet regions along the Greenland Ice Sheet 16

2.1 Top down view of NEMO horizontal mesh grid 28
2.2 ANHA4 horizontal mesh 29
2.3 ANHA12 horizontal mesh 29

3.1 Backward probability of 5 year transport of warm water 58
3.2 Backward depth of medium probability classification or higher 61
3.3 Forward probability of 5 year transport of surface water 65
3.4 Forward depth of medium probability classification or higher 69

Chapter 1

Background

1.1 Introduction

This chapter will go into the detail on some underlying topics. In order to understand the motivation behind our research questions for this thesis, there will be an introduction on the structure and ocean currents of the Arctic Ocean, Nordic Seas, Canadian Arctic Archipelago, Baffin Bay and the North Atlantic Ocean. The state of the Greenland Ice Sheet is discussed to fully provide additional context for this thesis and then discuss questions and thesis goals.

1.2 Geography and Currents of Arctic

The Arctic Ocean is bounded by multiple continental shelves: the Chukchi Shelf, the Alaska and Beaufort Shelf along North America that attaches to the Lincoln Shelf and then the Greenland Shelf, the European Shelf (Barents Shelf) and Siberian Shelf (Kara Shelf, Laptev Shelf, East Siberian Shelf). Ocean water exchanges occur through four gateways (three are visible in Figure 1.1): to the North Atlantic through bi-directional Fram Strait, Barents Sea to the Arctic and the Canadian Arctic Archipelago (CAA). As well there is inflow from the North Pacific via Bering Strait.

The Arctic Ocean water column is generally stratified with the upper water column being composed of Polar Surface Water, which can be separated into two classifications, the Polar Mixed Layer (PML) and the halocline, both overlying relatively warm and saline Atlantic water (Rudels, 2015). The upper water column may be affected by ice drift in the anticyclonic Beaufort Gyre located in the Beaufort Sea in the southern Canada Basin and along the Transpolar Drift from Siberia to Fram Strait (Rudels, 2015). The upper portion of the relatively warm Atlantic waters becomes homogenized in winter by thermal and haline convection and brine rejection as it enters the Arctic Ocean, contributing to the PML (Rudels, 2015). In the summer, the uppermost part of the PML is freshened by a seasonal melt layer, becoming stratified, which may be destroyed due to freezing during the fall (Korhonen *et al.*, 2013; Rudels, 2015).

The Arctic Ocean halocline, below the PML, has a strong salinity increase with depth, while the temperature remains close to freezing (Rudels, 2015). The Arctic Ocean halocline can be divided into two parts, the upper halocline and the lower halocline. The upper portion is derived from Bering Strait inflow and contains relatively warm Alaskan Coastal Water (31g/kg<S<32g/kg, $1^oC<T<6^oC$), Bering Sea Summer Water (32g/kg<S<33g/kg, $0^oC<T<2^oC$) and Bering Sea Winter Water as well as Siberian river waters (Korhonen *et al.*, 2013). The lower halocline contains cooler, dense waters (S$\sim$34g/kg) (Rudels, 2015).

The Atlantic water in the Arctic Ocean moves cyclonically around the continental margins, entering through Fram Strait (Beszczynska-Mőller *et al.*, 2012; Rudels, 2015). Fram Strait, located between eastern Greenland and west of Svalbard, provides the largest input of water, heat and salt into the Arctic Ocean by supplying the intermediate and bottom Arctic layers with Atlantic waters, stabilizing

the Arctic Ocean's stratification (Polyakov *et al.*, 2011; Spielhagen *et al.*, 2011; Bourgain & Gascard, 2012).

Atlantic waters pass the Greenland-Scotland Ridge and continues northward as the Norwegian Atlantic Current, which consists of its own two branches, one travelling through Fram Strait as the West Spitsbergen Current, and the other entering the Barents Sea (Beszczynska-Mőller *et al.*, 2012) (Figure 1.1). Temperatures of Atlantic waters in eastern Fram Strait vary between 2^oC to 6^oC, with salinities greater than 35 g/kg, and are found at intermediate depths of 50 metres to 600 metres (Spielhagen *et al.*, 2011). The upper portion of the Atlantic waters in the Fram Strait may melt sea ice and mix with fresher surface water of Arctic origin, transforming into a cooler, less saline surface layer, preserving the Atlantic water warm core below (Beszczynska-Mőller *et al.*, 2012).

Below 600 metres to about 800 metres, Atlantic waters temperatures are between 0^oC and 2^oC (Beszczynska-Mőller *et al.*, 2012). This characterization of Atlantic waters in Fram Strait is relatively warm and salty compared cold and fresh Arctic waters. The Atlantic layer in the Arctic can reach to depths of 900 metres, though temperatures are typically cooler, closer to 0^oC (Karcher *et al.*, 2011; Polyakov *et al.*, 2011).

Atlantic water will decrease in temperature as it moves away from Fram Strait due to diffusion processes and exchanges between surrounding colder Arctic water masses (Bourgain & Gascard, 2012). From Fram Strait across to the Beaufort Sea, the mean travel time of the intermediate Atlantic waters is around 15 years (Bourgain & Gascard, 2012) with a total of 30 years to return back to Fram Strait (Karcher *et al.*, 2011; Bourgain & Gascard, 2012). The presence of Atlantic waters in the Arctic Ocean may have an influence on surrounding water masses, which may affect sea ice distribu-

tion (Spielhagen *et al.*, 2011). Atlantic waters in the Arctic Ocean carry enough heat to melt the Arctic sea ice cover several times over (Polyakov *et al.*, 2011).

In Fram Strait, there is a portion of Atlantic Water that recirculates in the West Spitsbergen Current and returns south to the Nordic Seas (Karcher *et al.*, 2011; Beszczynska-Mőller *et al.*, 2012) (Figure 1.1). A part of this current flows south as cooled Arctic Atlantic Water in the East Greenland Current (EGC) (Rudels, 2015).

A portion of the Atlantic water is cooled as it travels into Barents Sea by: heat loss to the atmosphere, mixing with cold and dense water formed by ice formation and brine rejection Rudels (2015). The current continues northward into the Arctic Ocean, while the rest recirculates towards the Norwegian Sea (Rudels, 2015). A deep branch of Atlantic water that enters the Arctic Ocean through Fram Strait, continues as a boundary current and travels eastward along the continental slope (Rudels, 2015). As this current passes by the St. Anna Trough it mixes with the second inflow branch from Barents Sea, with relatively colder and less saline, inflow creating more layers (Rudels, 2015).

1.2.1 Warm Water Pulse

Atmospheric pressure fields, such as the North Atlantic Oscillation, and changes in ocean currents, are important for increasing the warming and presence of Atlantic waters in the Arctic Ocean (Karcher *et al.*, 2011; Beszczynska-Mőller *et al.*, 2012). Atlantic water decreases in temperature as it travels from Fram Strait into the Arctic Ocean due to lateral advection, eddy stirring, diffusion and upward heat transfer to the overlying, surface, waters (Polyakov *et al.*, 2011).

The strong positive state of the North Atlantic Oscillation, indi-

cated by strong westerly winds and a decrease in atmospheric heat input, led to the 1990s warming of Atlantic waters and increased volume inflow in the Arctic Ocean, mostly generated in the Nordic Seas (Karcher *et al.*, 2011; Spielhagen *et al.*, 2011; Beszczynska-Mőller *et al.*, 2012; Korhonen *et al.*, 2013). The warm pulse of Atlantic waters entered the Canada Basin during the 2000s, where the warm temperature anomalies cooled to 0.5^{o}C (Polyakov *et al.*, 2011).

During this event, the Atlantic waters propagated to shallow surfaces and the warm core of the Atlantic waters enhanced the heat flux to the surface waters (Spielhagen *et al.*, 2011). At the same time there was decreasing sea ice (Spielhagen *et al.*, 2011), suggesting that warm Atlantic may indeed have an impact on sea ice distribution in the Arctic Ocean. Though the link between the enhanced Atlantic waters and its overall affect on sea ice is still an open question.

The second Arctic warm water pulse entered the basin from 2004 to 2007 and was first observed downstream of Fram Strait in the eastern Eurasian Basin in 2004 (Polyakov *et al.*, 2011). The temperature anomalies for the Atlantic warm waters in the Arctic Ocean were up to 1^{o}C warmer and had a similar advection pattern to the 1990s event (Polyakov *et al.*, 2011). The peak of the second warming occurred when the anomalous warm Atlantic waters reached temperatures greater than 3^{o}C, through the increased northward advection of Atlantic waters due to the westward shift of the sub-arctic front and a contraction of the sub-polar gyre (Beszczynska-Mőller *et al.*, 2012).

Modelling done by Polyakov et al., (2011) suggests that the decrease in ice thickness in the Eurasian Basin over recent decades of about 30 centimetres is about equally due to an increase in Atlantic

heat flux and atmospheric thermodynamic forcing. This shows the importance that oceanic heat can have on the cryosphere and should be taken into account, along with atmospheric influence.

1.2.2 Canadian Arctic Archipelago

The CAA is a combination of multiple networks of straits, basins (125 to 230 metre depth) and narrow channels (1 to 10 km) connecting the Arctic Ocean to the northwest Atlantic Ocean (Rudels, 2015). In order to adequately reflect the important influence of topography in the CAA, ocean circulation models need to have adequate resolutions in this region.

In the Arctic region, there are a few characteristics that can directly impact the transport of the flow such as sea ice, wind events and sea-level elevation (Aksenov *et al.*, 2010). Different sea ice features can affect the ocean dynamics, such as ocean surface currents, and ice (solid) freshwater transport. Sea ice can vary between being land-fast and mobile. Fast-ice can create a buffer between wind surface currents and the forcing effect on surface currents. Therefore a coupled ocean-ice dynamic model provides more information than just an ocean dynamic model, and therefore will produce better estimates of flux transport.

Arctic waters can travel through the CAA into Baffin Bay through: Nares Strait, Barrow Strait, Cardigan Strait- Hell Gate,joining Arctic waters exported via Hudson Strait, continuing to the Labrador Sea through the 640 metre deep Davis Strait (Figure 1.1) (Aksenov *et al.*, 2010; Rudels, 2015).

1.3 Baffin Bay

Baffin Bay, between Baffin Island and Greenland (Figure 1.1), has a cyclonic gyre, which receives its freshwater from the CAA, and the West Greenland current (WGC) (Melling *et al.*, 2008; Myers *et al.*, 2009) which feeds the east branch of the Baffin Bay gyre. The CAA straits are too shallow to let the dense Atlantic layer pass through into Baffin Bay, therefore the warm layer in Baffin Bay must enter from the south through Davis Strait (Rudels, 2015). The warmest and most saline waters are from the WGC on the east side of the basin (Melling *et al.*, 2008). The salinity of the warm layer is relatively low (34.5 g/kg), containing mixed Irminger Current water (with Polar water from EGC before continuing into WGC into Baffin Bay) (Rudels, 2015).

Below 1000 metre depth, Baffin Bay has dense waters that are below the sill depth of Davis Strait (Gladish *et al.*, 2015). With Baffin Bay at 300 to 800 metres depth, the West Greenland Intermediate Water which enters as warm WGC water cools as it circulates Baffin Bay (Gladish *et al.*, 2015). Overlaying the warmer Baffin Bay intermediate water is the Baffin Bay thermohaline water (Gladish *et al.*, 2015). Subsurface Baffin Bay Arctic Water enters through the CAA with temperature minimum and low salinity (Gladish *et al.*, 2015).

The intermediate layer of the WGC carries warm, modified, Irminger Water, which are relatively warmer and saltier (Melling *et al.*, 2008), northward along the west Greenland shelf in Baffin Bay. Observations showed that warm, subsurface waters reached the mouth of the Jakobshavn ocean fjord at the time of rapid thinning and retreat of this glacier (Holland *et al.*, 2008). It was seen that warm subsurface waters were carried beyond the sill and up to the fjord (Holland *et al.*, 2008).

The freshwater released from the northwest of the Greenland Ice Sheet (GrIS) enters directly into Baffin Bay and likely decreases the salinity at the surface layers. Castro de la Guardia (2015) found that with increased melt runoff from the northwest section of the GrIS, there was an increase in sea surface height along the west coast of Greenland which resulted in strengthening the WGC.

1.4 North Atlantic Subpolar Gyre

The North Atlantic Current (NAC) forms the southern part of the North Atlantic Subpolar Gyre (NASPG) (Figure 1.1). At depths above 1000 metres in the NAC, relatively warm (8^oC to 15^oC), saline (35 g/kg to 36 g/kg) thermocline waters pass by the Grand Banks and travel to the West European Basins (Fratantoni & Pickart, 2007).

The Irminger Current is formed when part of the NAC separates and circulates along the Reykjanes Ridge (Fratantoni & Pickart, 2007). The Irminger Current typically travels along southeast Greenland where it merges with the EGC, rounding Cape Farewell and subducting under the low-salinity polar water, forming the WGC (Straneo, 2006; Fratantoni & Pickart, 2007; Melling *et al.*, 2008; Myers *et al.*, 2009). Along Greenland's eastern shelf, the East Greenland Coastal Current (EGCC) travels past Cape Farewell, carrying very fresh polar waters, as well as Greenland melt (Bacon *et al.*, 2014).

Local melting of sea ice exported through Fram Strait is a dominant contributor to the freshwater content of the EGCC (Bacon *et al.*, 2014), though due to the proximity of the GrIS, there must be some contribution from the ice sheet. It is the heat content available from the Irminger Current and EGC that may influence the

total FWF of a marine terminating glacier on northwest Greenland (Holland *et al.*, 2008; Myers & Ribergaard, 2013).

WGC separates into two branches: one travels northward along the west coast of Greenland into Baffin Bay (as mentioned above in Section 1.3), bringing with it both less saline, cold Polar water and relatively warm, saline, modified Irminger Sea water (Myers *et al.*, 2009) and the second, warmer and more saline branch joins the southward flowing Baffin Island Current at Davis Strait (Fratantoni & Pickart, 2007). As mentioned in Section 1.3, with increased GrIS melt into Baffin Bay, the gyre may strengthen, which may lead to an increase in presence of the WGC, which may have a direct response to the mass loss rate on the west side of the GrIS (Myers *et al.*, 2009)

The west branch of Baffin Bay circulates cold waters southwards through Davis Strait, accompanied by the outflow through Hudson Strait (Fratantoni & Pickart, 2007), into the Labrador Current, where freshwater may circulate in to the Labrador Sea (connected to the west of the NASPG, defined by the 3300 metre isobath (Straneo, 2006)) (Melling *et al.*, 2008). There are many sources of freshwater that enters the NASPG: river runoff, waters from the Arctic Ocean, sea ice, icebergs, and the GrIS being the largest reservoir for freshwater (Dickson *et al.*, 2007).

The Labrador Sea has significant biological activity, intense air-sea interactions, extreme winds, cold temperatures, icebergs and sea ice (Marshall *et al.*, 1998). Buoyancy-driven convection occurs in the Labrador Sea (Myers *et al.*, 2009), this deep water formation links to the North Atlantic Deep Water (NADW) current (Weijer *et al.*, 2012). Buoyancy-driven convection may be sensitive to heat loss and freshwater input the central Labrador Sea, as one will drive deep convection and the other, lower the density of the surface wa-

ters, slowing down convection (Aagaard & Carmack, 1989; Straneo, 2006; Weijer *et al.*, 2012).

There are two distinct periods in the Labrador Sea, restratification and convection (Straneo, 2006). The extent of the Labrador Sea mixed layer depth changes seasonally due to air-sea heat fluxes and layered restratification. During the restratification process (May to December), the surface layer of the water column undergoes a freshening and a warming, with an increase in salt content in the lower layer (Straneo, 2006). During the convective process (January to April), the mixed layer deepens into the lower layer of the water column, and the trends from the previous process is reversed.

The NADW makes the deep branch of the Atlantic Meridonal Overturning Circulation (AMOC), therefore changes in the rate of convection at the Labrador Sea may have an impact on the AMOC (Dickson *et al.*, 2007; Weijer *et al.*, 2012). The AMOC is responsible for northward heat transport in the upper ocean waters, and deep southward flow of cold water, and therefore has a strong influence for our climate system (Dickson *et al.*, 2007; Weijer *et al.*, 2012).

In recent years, there has been discussions on how GrIS enhanced melt may affect ocean circulation (Fichefet *et al.*, 2003; Swingedouw *et al.*, 2014). The sensitivity of the AMOC to FWF varies depending on different climate model simulations, though they come to the same result, with increased FWF from the GrIS the AMOC will go undergo a weakening phase (Fichefet *et al.*, 2003; Swingedouw *et al.*, 2014). A slowdown of this circulation and its heat transport could have a significant impact on how the earth regulates its temperatures (Straneo & Heimbach, 2013).

1.5 Enhanced Greenland Melt

The GrIS's mass loss has accelerated over recent years (Box *et al.*, 2006; Rignot & Kanagaratnam, 2006; Van Den Broeke *et al.*, 2009; Shepherd *et al.*, 2012) with the freshwater anomaly, since 1995, reaching around $\frac{1}{3}$ of the amount of the 1970s Great Salinity Anomaly (Bamber *et al.*, 2012). Within a 20 year period the mass balance estimates have quadrupled from -51 +/- 65 Gt/year during 1992 to 2000, to -211 +/- 37 Gt/year during 2000 to 2011 (Shepherd *et al.*, 2012) and melting period had also lengthened (Box *et al.*, 2006).

The GrIS contributed to 6.1 mm/decade of sea level rise from the period of 2002 to 2010 (Fichefet *et al.*, 2003). As mentioned in Section 1.4, freshwater may slowdown ocean convective systems (Aagaard & Carmack, 1989). Experiments of enhanced GrIS show weakening of the North Atlantic thermohaline circulation by the end of the 21st century (Fichefet *et al.*, 2003).

Suggested causes of mass loss from the GrIS include: increased surface air temperatures (Rignot & Kanagaratnam, 2006; Hanna *et al.*, 2013; Straneo & Heimbach, 2013), the positive feedback from the decrease in Arctic sea ice impacting polar temperatures (Hanna *et al.*, 2013), warmer ocean temperatures around Greenland (Rignot & Kanagaratnam, 2006; Holland *et al.*, 2008; Myers & Ribergaard, 2013; Straneo & Heimbach, 2013; Jackson *et al.*, 2014), and the fluctuation of heat content in the NASPG (Myers & Ribergaard, 2013; Holland *et al.*, 2008). In non summer months, atmosphere temperatures are low and therefore glacial melt has a large dependency on the externally forced ocean exchanging onto the Greenland shelf towards the ice sheet's glaciers (Jackson *et al.*, 2014).

There has been an increased presence of warmer waters in fjords

of fast-moving marine terminating glaciers such as Jakobshavn in Disko Bay (Holland *et al.*, 2008; Myers & Ribergaard, 2013), and south east glaciers, Helheim (Sermilk Fjord) and Kangerdlugssuaq (Kangerdlugssuaq Fjord) (Christoffersen *et al.*, 2011; Sutherland *et al.*, 2014), which occurred at the time these marine terminating glaciers retreated (Holland *et al.*, 2008; Myers & Ribergaard, 2013; Christoffersen *et al.*, 2011).

Oceanic circulation may affect total freshwater flux by the role that oceanic heat can play on the ice sheet (Holland *et al.*, 2008; Myers & Ribergaard, 2013; Straneo & Heimbach, 2013; Jackson *et al.*, 2014). As previously discussed, the warm modified Irminger waters travel along the WGC into Baffin Bay, it is the heat content available from this water mass that may influence the total FWF of a marine terminating glacier on GrIS (Straneo & Heimbach, 2013; Myers & Ribergaard, 2013; Straneo *et al.*, 2012; Holland *et al.*, 2008). The warmest Atlantic water near the GrIS is found near the southeast and then the northwest and central-west sectors of Greenland (Straneo & Heimbach, 2013; Straneo *et al.*, 2012). The northern sectors of the GrIS are bounded by cool polar waters and oceanic heat may not play an important role in that region of GrIS (Straneo & Heimbach, 2013; Straneo *et al.*, 2012). The northwest and southeast sectors of GrIS account for 80% of the ice sheet's discharge (Enderlin *et al.*, 2014). Both regions have experienced the largest increase in total FWF from the 1990s to 2010 (Bamber *et al.*, 2012), a time where NASPG waters were a record high due to the slow down of the gyre (Straneo & Heimbach, 2013).

How the Atlantic and Arctic water layers in a glacial fjord existed in the past, and how they will change in the future may have a significant influence on the floating extension of the grounded ice wall terminating in a marine glacier (Jenkins, 2011; Straneo *et al.*,

2011).

1.6 Thesis Questions

The way the research was conducted for this Masters project was to make use of previous model runs and experiments completed in the laboratory. Using previous experiments led to an an introduction and familiarization with ocean models and the techniques involved with the parameterizations included in different configurations. I also learned how different approaches can affect the result, or help to look at specific questions.

This thesis aims to answer two questions: to find the source of the warm waters approaching the marine terminating glaciers of the GrIS. And then, where the freshwater, once released into the ocean is taken up by the oceanic circulation surrounding Greenland.

We explore and classify the pathways for the warmer Atlantic waters that reach the fjords along the coasts of Greenland. Additionally, given that the melt of these glaciers is accelerating, we look at the pathways of the low salinity melt waters from these coastal glaciers and where it is taken up in the surrounding basins. This analysis is carried out using an Arctic and North Hemisphere Atlantic configuration of the NEMO ocean/sea ice general circulation model (Madec, 2008) run at both $\frac{1}{4}^o$ and $\frac{1}{12}^o$ resolution. Pathways are determined using the ARIANE Lagrangian float package (Blanke & Grima, 2008) using both forward and reverse trajectory analysis and can be ran offline. Running an experiment online take time, on the scale of months. Therefore, using the experiments previous ran and applying an offline tool worked well with the time span of a masters thesis.

The research questions were targeted by first learning about

the ocean and the GrIS. The GrIS has many marine-terminating glaciers. To focus this project, I isolated 13 outlet regions (locations where the marine-terminating glaciers melt into) distributed along the entire coast of Greenland (Figure 1.1, where previous literature discussed the largest ice loss, with the highest contribution to the freshwater content into the oceans (Rignot & Mouginot, 2012; Straneo *et al.*, 2011, 2012; Myers & Ribergaard, 2013). At each outlet region, we examined the water properties of the water column. This let us find the range of temperature and salinity and the corresponding depth for particle insertion.

As said above the 13 outlet regions I have focused on are picked due to the acceleration of the glaciers in that region. In the north we have Petermann Glacier (PG), one of the fastest glaciers in this area (Rignot & Mouginot, 2012). The section from Kong Oscar to Illullip Sermia (KO2I) is located in the north west and is close to several fast marine terminating glaciers: Kong Oscar, Nansen and Sverdrup Glacier (Rignot & Mouginot, 2012).

In the centre west we have 3 different outlet regions, as fast moving glaciers are common in the north west and centre west regions (Rignot & Mouginot, 2012). The bay north of Sullorsuaq (NSULL) holds freshwater export from the Rink and Store marine terminating glaciers. The outlet region of Sullorsuaq (SULL) covers the northern export from Disko Bay. Then I have the outlet region of Disko Bay (DB). These last two outlet regions cover freshwater flux coming from marine terminating glaciers such as Jakobshavn Isbrae, the fastest moving glacier on the GrIS (Rignot & Mouginot, 2012).

In the southwest, in the outlet region Nuuk (NU), the glaciers are not as fast as the ones in the north, but they still have relatively high velocities (Rignot & Mouginot, 2012). The section in the south,

closest to the warm Atlantic waters, includes the glaciers around Julianehab (JUL) (Straneo & Heimbach, 2013; Straneo *et al.*, 2012).

On the southeast of Greenland, Helheim Glacier (HEL), as well as Kangerdlugssuaq Glacier (KGLQ) exports from the second largest ice cap, Hutchinson Plateau (Rignot & Mouginot, 2012). Kong Christian IV glacier drains one third of the largest ice cap in Greenland (Geikie plateau and Watkins Bejerge) (Rignot & Mouginot, 2012). The Scoresby Sund holds the export of one of the fastest-moving glaciers, Daugaard-Jensen (Rignot & Mouginot, 2012). The two outlets are used for the North East sector of Greenland are Zachariae Isstrom (ZI) and Nioghalvfjerdsfjorden (79NG). Mass loss has accelerated on ZI while 79NG has been stable (Rignot & Mouginot, 2012).

Previous work has looked at identifying warm Atlantic waters by marine terminating glaciers on the GrIS (Holland *et al.*, 2008; Jenkins, 2011; Straneo *et al.*, 2012; Myers & Ribergaard, 2013; Straneo & Heimbach, 2013; Inall *et al.*, 2014; Jackson *et al.*, 2014). Straneo (2011) identified warm Atlantic water near the Helheim Glacier for the summer and winter seasons. Straneo (2012) found the warmest (deep) AW is found near HEL and DB followed by KGLQ and 79NG, with PG having the coldest warm Atlantic Water. Their study showed that while the Atlantic Waters may take different routes since there is some variability in water temperature, and the authors were not able to identify the actual routes taken by the warm water. It still remains a question about the differences in heat transport between Helheim and Kangerdlugssuaq Glaciers.

We hoped to classify the GrIS glacier's warm source waters, as in these waters have enough heat to increase and maintain melt from the marine terminating glaciers. We also wanted to know if we can see where the GrIS's marine terminating glacier's freshwater enters

the ocean, and what region of the ocean may then be effected by this influx of buoyant waters.

1.7 Figures

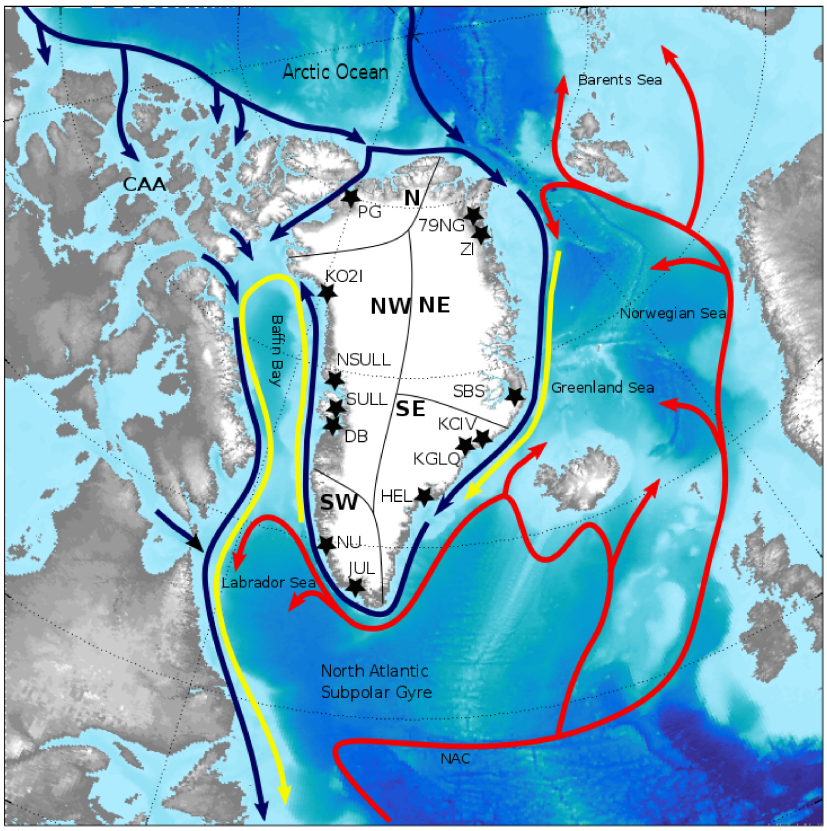

Figure 1.1: Ocean Circulation around Greenland and 13 outlet regions along the Greenland Ice Sheet. Atlantic waters are seen in red, as they travel from the North Atlantic Current northward, separating into two branches, one along Reykjanes Ridge and the other through the Greenland-Scotland Ridge. The first branch continues along south east Greenland, mixing with the West Greenland Current, heading into Baffin Bay and continuing south through Davis Strait with the Baffin Bay current. The Greenland-Scotland Atlantic water continues to travel north, entering the Arctic Ocean through Fram Strait as the West Spitsbergen Current or through Barents Sea. The yellow currents represent the mixed and cooled Atlantic waters, as they get recirculated in Fram Strait and continue with the East Greenland Current as well as the Atlantic water mixes with the West Greenland Current that enters Baffin Bay. Arctic water and freshwater pathways are shown in blue. Arctic waters enter the North Atlantic through Fram Strait, which contributes to the East Greenland Current and is transported along the shelf into Baffin Bay where it will exit south through Davis Strait through the Baffin Bay Current in to the Labrador Current. Arctic water can also enter through the Canadian Arctic Archipelago through Nares Strait, Barrow Strait, Cardigan Strait- Hell Gate and Hudson Strait. This image shows the distribution of the 13 outlet regions examined along the coast of the Greenland Ice Sheet and the sectors they are found in, north (N), north west (NW), south west (SW), south east (SE), and northeast (NE). For exact locations see Table 2.3.

Chapter 2

Numerical Methods

2.1 NEMO

We used a primitive equation, eddy permitting, system of numerical models, Nucleus for European Modelling of the Ocean (NEMO) version 3.4, to examine pathways of GrIS melt, as well as source the warm waters found near marine terminating glaciers. To represent sea ice, NEMO is interfaced with a sea ice thermodynamic and dynamic numerical model, the Louvain la-neauve Ice Model (LIM2) (Fichefet & Morales Maqueda, 1997; Madec, 2008). The ocean engine, Ocean Parallelise (OPA), is used for ocean dynamics and thermodynamics on a three dimensional Arakawa C-type staggered grid.

We compared 3 different experiments with a regional Arctic Northern Hemisphere Atlantic (ANHA) configuration: a $1/4^o$, ANHA4 reference run and ANHA4 with additional runoff (Dukhovskoy *et al.*, submitted) and $1/12^o$ ANHA12, hereinafter called ANHA4REF, ANHA4RUNOFF and ANHA12, respectively.

The domain of the high-resolution output from the ANHA configuration covers the whole Arctic Ocean, North Atlantic and part of South Atlantic, with two open boundaries: one at Bering Strait and the other at 20^oS (Dukhovskoy *et al.*, submitted). The config-

uration's mesh grid is extracted from a global configuration on a tripolar grid, ORCA (DRAKKAR *et al.*, 2007).

Initial conditions were provided by Global Ocean Reanalyses and Simulations (GLORYS1v1) which include: temperature, salinity, sea surface height and horizontal velocities (zonal and meridonal) as well as monthly open boundary conditions for the same fields (Ferry *et al.*, 2008). The reanalysis forecast error covariance, used in GLORYS, is based on statistics of a collection of 3 dimensional ocean state anomalies with seasonal variability (Ferry *et al.*, 2008). GLORYS uses a total variation diminishing (TVD) scheme with enstrophy and energy conserving scheme for the advection scheme and bilaplacian iso-level diffusion and Laplacian diffusion operator (Ferry *et al.*, 2008). The ocean initial condition in temperature and salinity is based on ARIVO global climatology with the first three months considered as a spin-up of GLORYS-1 system (Ferry *et al.*, 2008). The initial ice field is a combination of ice concentration and ice thickness (provided by satellite observation and GLORYS1v1 respectively).

The LIM2 ice model assumes that ice behaves as an elastic viscous plastic dynamical system to include the interaction of the stress between ocean and ice computed at each time step (Fichefet & Morales Maqueda, 1997; Ferry *et al.*, 2008).

Fields were taken from GLORYS1 (2002 to 2007) and GLORYS2 (2008-2010) in the ANHA configuration (Ferry *et al.*, 2012). For ANHA configuration, the atmospheric forcing data, provided by Canadian Meteorological Centre's (CMC) global deterministic prediction system (GDPS) reforcasts (CGRF) dataset (Smith *et al.*, 2014) has hourly 33km resolution for the following fields: 10 metre surface wind, 2 metre air temperature and humidity, downward shortwave and longwave radiation and total precipitation. From the

total precipitation, snowfall is represented when temperature at the surface is greater than 0^oC, and rain otherwise (Hu, 2015, personal communication). Snowfall is provided by the inter-annual Coordinated Ocean Research Experiments (CORE) v2 dataset (Large & Yeager, 2008).

Primitive equations based on the Navier-Stokes equations, along with a nonlinear equation of state couples two active tracers (temperature and salinity) to the fluid velocity. For scale considerations, the following assumptions are made:

1. Spherical Earth Approximation: Geopotential surfaces are assumed to be spheres so that gravity is parallel to the Earth's radius

2. Thin-Shell Approximation: Since the ocean depth is smaller than the Earth's radius, ocean depth is neglected compared to the Earth's radius

3. Turbulent Closure Hypothesis: Turbulent fluxes that represent small scale processes that effect large-scale processes, are expressed in terms of large-scale features

4. Boussinesq Hypothesis: Density contributes to the buoyancy force and are neglected in any other case

5. Hydrostatic Hypothesis: Removal of convective processes from initial Navier-Stokes equations and parameterization of convective processes. The vertical momentum equation is balance between the vertical pressure gradient and buoyant force

6. Incompressibility Hypothesis: Three dimensional divergence of the velocity vector is assumed to be zero

Model Basics:

The vector invariant form of the primitive equations on an (i,j,k) vector system provides the following seven equations (namely the momentum balance, hydrostatic equilibrium, the incompressibility equation, the heat and salt conversion equations and an equation of state:

$$\frac{\partial \vec{U_h}}{\partial t} = -\Big[(\nabla \times \vec{U}) \times \vec{U} + \frac{1}{2}\nabla(\vec{U}^2)\Big]_h - fk \times \vec{U_h} - \frac{1}{\rho_o}\nabla_h p + D^{\vec{U}} + F^{\vec{U}} \quad (2.1)$$

$$\frac{\partial p}{\partial z} = -\rho g \quad (2.2)$$

$$\nabla \cdot U = 0 \quad (2.3)$$

$$\frac{\partial T}{\partial t} = -\nabla \cdot (TU) + D^T + F^T \quad (2.4)$$

$$\frac{\partial S}{\partial t} = -\nabla \cdot (SU) + D^S + F^S \quad (2.5)$$

$$\rho = \rho(T, S, p) \quad (2.6)$$

where $\vec{U}$ is the vector velocity (U,V), ∇ is the generalized derivative vector operator in (i,j,k) directions, t is the time, z is the vertical coordinate, ρ is the insitu density given by equation of state (2.6), ρ_o is a reference density, p is the pressure, f=$2\vec{\Omega} \cdot$ k is the Coriolis acceleration, where $\vec{\Omega}$ is the Earth's angular velocity vector, and g is the gravitational acceleration. D^U, D^T and D^S are parameterizations of small-scale physics for momentum, temperature and salinity, and F^U, F^T and F^S surface forcing terms.

The boundary conditions are set by the ocean bounded with bottom topography at its base and air-sea or ice-sea interfaces at the top. z=-H(i,j) and z=η(i,j,k,t) where H is the depth of the sea floor and η is the height of the sea surface, with reference to z=0.

The land-ocean interface has a mass exchange between continental margins and ocean through river runoff. This exchange can modify the sea surface salinity. The solid earth-ocean interface exchanges heat and fluxes through the sea floor, which are small and typically can be neglected in the model. Although, geothermal heating, which is associated with solid Earth cooling, may have an impact on the thermohaline circulation of the ocean (Madec, 2008). The boundary condition is set for no flux exchange of heat and salt across the solid boundaries. For momentum, the bottom velocity is parallel to the solid boundaries. Kinematic boundary conditions are expressed as:

$$w = -U_h \cdot \nabla_h(H) \tag{2.7}$$

The atmosphere-ocean interfaces exchanges horizontal momentum of wind stress and heat. The kinematic surface condition and mass flux of fresh water budget (precipitation minus evaporation), leads to:

$$w = \frac{\partial \eta}{\partial t} + U_h|_{(\mathrm{z=n})} \cdot \nabla_h(\eta) + P - E \tag{2.8}$$

At this dynamic boundary condition, there is a removal of capillary waves from the system by neglecting surface tension, leading to a continuity of pressure across the interface z=η. The sea ice - ocean interface exchanges heat, salt, fresh water and momentum. At this interface the sea surface temperature is set to be at the freezing point with sea ice salinity relatively low (around 4 to 6 g/kg) compared to that of the ocean (34 g/kg).

For the pressure formulation, the total pressure at a given depth z is composed of a surface pressure p_s at a reference geopotential surface (z=0) and a hydrostatic pressure p_h. The configuration used in this study used the free surface formulation for the surface pressure term. The free-surface elevation, η, describes the shape

of the air-sea interface and involves of the excitation of external gravity waves.

With barotropic flow and the surface as a restoring force as it moves up and down, the phase speed of these waves are high, and thus the model uses time-splitting and a short barotropic time step.

Effects of smaller scale motions must be represented entirely in terms of large-scale patterns to complete the equations. This is important for long-term simulations as small scale processes are important in balancing kinetic energy and heat. These affects appear in the primitive equations as the divergence of turbulent fluxes.

In order for the experiments used in this study to simulate lateral eddy fluxes, it is important on whether the size of the eddies is below or above the grid-spacing. For the eddy resolving configuration used in this study, ANHA12, a second order operator can be used, but usually a more scale selective one (biharmonic operator) is preferred as the grid-spacing is usually not small enough compared to the scale of eddies.

Subgrid scale physics increases the stability of the model by dissipating the energy towards the grid scale and not interfering with the solved mesoscale activity.

The three dimension Arakawa C-type staggered grid (Figure 2.1) holds the arrangement of variables consistent in all directions. Cells of the grid are centred on scalar points (T,S,p,ρ) with vector points (u,v,w) defined in the centre of each cell. The ocean mesh is defined the transformation that gives (λ,φ,z) as a function of (i,j,k). The grid-points are located at integer or integer and a half value of (i,j,k).

As mentioned above, the configuration used in this study, ANHA, had a pre-built horizontal mesh grid (global ORCA mesh grid (DRAKKAR *et al.*, 2007) that NEMO reads in. The vertical coordinate of the model uses a z-coordinate with partial step bathymetry.

The vertical grid is computed in the code from the bathymetry. The model mesh is determined by four things: bathymetry given in metres, number of levels of the model, an analytical transformation and the vertical scale factors and the masking system (ie. number of model levels at each (i,j) column). Where usually the bathymetry is built by interpolating a standard bathymetry product onto the horizontal ocean mesh, instead NEMO reads in a bathymetry file (file that provides the ocean depth, positive in metres) at each grid point of the model grid. ANHA has 50 levels with layer thickness increasing from 1.05 metres at the surface to 453.13 metres and at the bottom partial steps are used. To defined coastlines, the bathymetry is set to zero and no model levels are defined.

Experiments using the Arctic Northern Hemisphere Atlantic Configuration

The experiments used here have been structured and set up by Paul Myers' Geophysical Fluid Dynamics Ocean Modelling Group at the University of Alberta in the Earth and Atmospheric Sciences Department (http://knossos.eas.ualberta.ca/xianmin/anha). Full details on the configuration is listed in Table 2.4. All of the reference experiments (ANAH4REF and ANHA12) include the total runoff into regions on the ocean grid by direct interpolation (on the fly) by NEMO's bilinear interpolation of Dai and Trenberth $1^o \times 1^o$ gridded monthly climatology. The ANHA4RUNOFF experiment includes the Greenland meltwater (Bamber *et al.*, 2012) (a volume conserving, resolution independent, directionally distributed runoff data field) applied onto the ocean model grid (Remap-II) (Dukhovskoy *et al.*, submitted).

1. ANHA4REF

   ANHA at $\frac{1}{4}^o$ horizontal grid framework comes from ORCA025

(DRAKKAR *et al.*, 2007), resolution ranges from ∼5.79km northern Canada and ∼27.9km at the equator. Runoff data is interpolated from a $1^o \times 1^o$ global monthly climatology dataset (Dai *et al.*, 2009). See Figure 2.2.

2. ANHA4RUNOFF Is the same set up as ANHA4REF except runoff is monthly climatology with Greenland melt (Bamber *et al.*, 2012) (remap-II) (Dukhovskoy *et al.*, submitted). This method provides more accurate runoff input to reduce the salinity drift in the experiment. See Figure 2.2.

3. ANHA12

   The $\frac{1}{12}^o$ horizontal resolution, has a resolution of ∼1.93km near the artificial pole over northern Canada and ∼9.3km at the equator. Runoff data is interpolated from a $1^o \times 1^o$ global monthly climatology dataset (Dai *et al.*, 2009). See Figure 2.3.

2.2 Trajectory Calculation

The offline Lagrangian tool that uses model output velocity fields as an input, ARIANE (Blanke & Raynaud, 1997), is used on our NEMO simulation. ARIANE's diagnostics are based on the calculation of multiple trajectories to integrate particle trajectories in the three dimensional modelled velocity field (Blanke & Raynaud, 1997). Calculations are with time, moving forwards or backward, fitted to the nature of the ocean circulation (Blanke & Raynaud, 1997). This method for computing a trajectory is fast and accurate as it only calculates positions on the edge of individual grid cells, offline, not having to be run with the model (Blanke & Grima, 2008).

ARIANE has a namelist that checks the particularities of the

model grid that is read. We have set ARIANE to not read all the data at once by setting a sequential parameter, therefore the interpolation is done in space (Blanke & Grima, 2008). ARIANE has the option to run a qualitative or quantitative experiments (Blanke & Grima, 2008). In our study we ran the former to fully monitor the successive positions, where quantitative would evaluate the mass transport between the initial and final location (Blanke & Grima, 2008). We set ARIANE to account for the partial cell depths as well as vertical integration of the divergence from the horizontal movement. By default ARIANE applies an upward integration from the flow of the ocean bottom (vertical velocity equals zero) to the surface (Blanke & Grima, 2008). The integration of vertical velocity can cause an error at the surface of nonzero values, such that particles will enter the atmosphere.

ARIANE also allows backward integration, which can be performed to track the origin of a given region of water (Blanke & Grima, 2008). ARIANE provides an estimate of transport with particles whose initial positions are homogeneously distributed in space and time (Blanke & Grima, 2008). Particles evolve based on the Eulerian output fields (temperature, density and salinity), however certain process cannot be resolved from the Lagrangian calculations, e.g. diffusion and convective mixing. The Eulerian output fields from the ocean model include the parameterization of such process in the ocean tracer and dynamic fields. Therefore, ARIANE should produce a reliable representation of tracer movement.

2.2.1 Backward Trajectory Analysis

Backwards integration for the same 13 outlet regions (Table 2.3) was done to find each location's warm water source by releasing 5000 particles throughout the entire water column. We examined

a specific water mass where temperature and salinity are that of the warm water sourced from the Irminger Sea. See Table 2.2 for definitions of temperature and salinity per region. Each region required an individual analysis to search for the water mass that was relatively saline with temperatures greater than 0^{o}C. When possible, the salinity criteria was increased to capture the most saline and relatively warm, water mass.

2.2.2 Forward Trajectory Analysis

To simulate how the surface waters at each outlet region get taken up by the surrounding ocean currents, about 1000 initial positions were initialized in the first 21 model grid level of the water column (77.85 metres) and then the Lagrangian calculations done by the ARIANE offline tracking tool over a 5 model year run by moving forward in time.

2.3 Analysis

To analyze our results, we have two separate tasks; backwards integration and forward integration from our outlet regions.

The analysis was done using the output (5 day) velocity fields for years 2002-2010 for ANHA4 and ANHA12 for each outlet region to examine the pathways and how they evolved through the forward and backward integration. We examined the pathways the virtual float followed in our horizontal grid. To set a probability, the total occurrences in a grid cell is divided by the total occurrences for a float in all grid cells for all years. ARIANE was initiated at a specific time with initial positions set by our 13 outlet regions (Table 2.3) and the tracers recorded the positions along their trajectories for 5 years. For our forward calculations, the start time for all ex-

periments is the beginning of each year (e.g. January 5th, 2002, January 5th, 2003, January 5th, 2004, January 5th, 2005, January, 5th 2006), and then run for 5 years forward in time. For the backward calculations, the initial start time for all experiments was at the end of each year (e.g. December 30th, 2010, December 30th, 2009, December 30th, 2008, December 30th, 2007, December 30th, 2006) and then run for 5 years backwards in time.

We plotted the 5 year average for all 13 locations, backward and forward integration. Results showed the likelihood that a particle was contained in a grid cell in our configuration. This was done by looking at the total number of particles throughout the 5 year offline run, and how many times a particle entered the grid cell. From the calculated values, we got a quantitative measurement of warm water sources and thus how the freshwater content may be taken up into the ocean.

Probability terms are defined in Table 2.1. These values correspond to the percentage that out of all floats and grid cells, the percentage that one parcel (as defined by the specific parameter of temperature and salinity) was contained in that grid during the 5 year simulation.

2.4 Figures and Tables

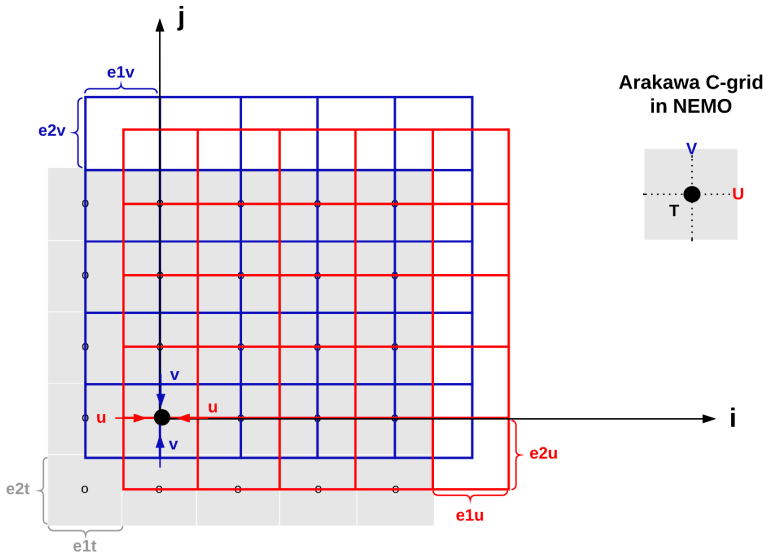

Figure 2.1: Top down view of NEMO horizontal mesh grid (Arakawa C-grid): This staggered grid holds the arrangement of variables in all directions. Cells of the tracer (scalar) points (T, s, p, ρ) is displayed on the gray grid. The tracer is always at the centre of this grid. Shown as the black filled circle. The vector points are (u,v). The u grid is shown in red, with an offset to the right u(i+1/2,j) and v grid is shown in blue, with an offset above v(i,j+1/2). A close up of the cell is shown in the subset to the right of the grid. Values of e are the length of each grid (ie. e1t, e2t is the grid cell length in i and j).

Table 2.1: Percentage Definition: Terminology used to classify the percentage that a float is contained in a given grid cell.

Probability Terms	Percentages
Very High	1 to $1e^{-}1$
High	$1e^{-}1$ to $1e^{-}2$
Medium	$1e^{-}2$ to $1e^{-}3$
Low	$1e^{-}3$ to $1e^{-}4$
Very Low	$1e^{-}4$ to $1e^{-}5$

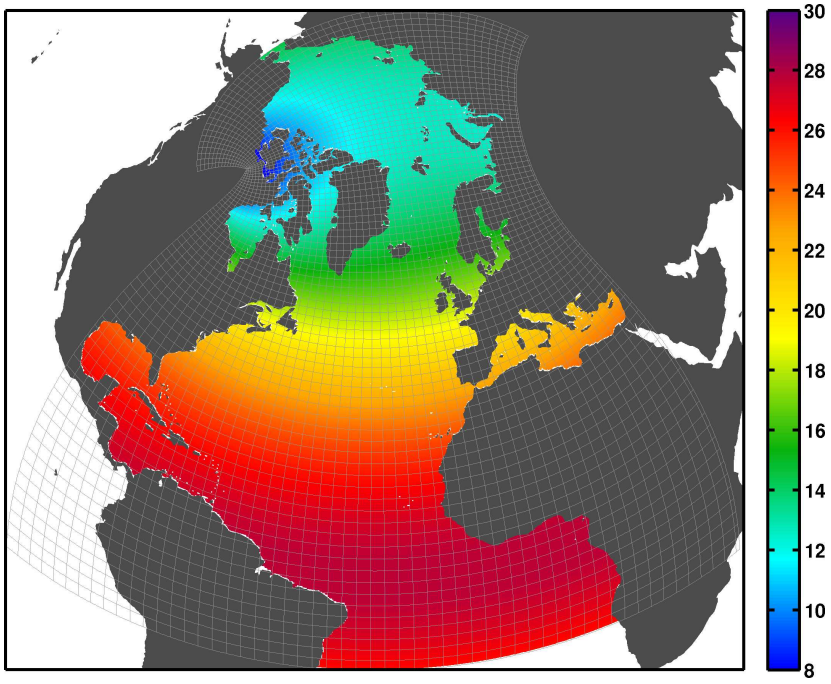

Figure 2.2: ANHA4 horizontal mesh (every 10 grids, colour shows the resolution in kilometres).

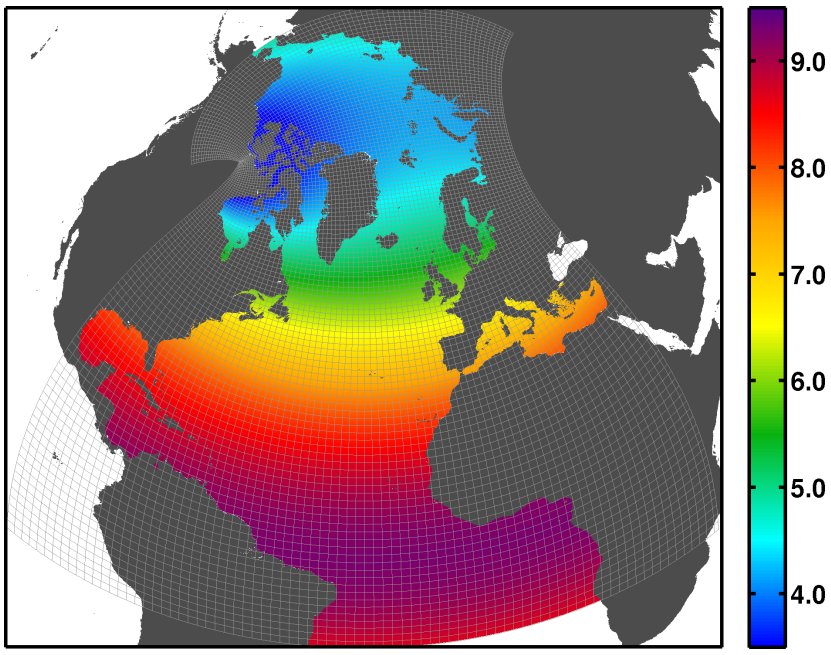

Figure 2.3: ANHA12 horizontal mesh (every 20 grids, colour shows the resolution in kilometres).

Table 2.2: Definition of the relatively warm, saline waters that are found by the outlet regions (Table 2.3). These are the values that we use to define the trajectories to include in Figure 3.1 and Figure 3.2 with ARIANE for the backward trajectory analysis.

Temperature (^{o}C)	Salinity	Region
0.0	34.1	ZI, 79NG
0.2	34.1	PG, KO2I, NSULL, KGLQ, KCIV
0.2	34.5	SULL, DB
0.2	34.7	NU, SBS
0.2	34.88	JUL, HEL

Table 2.3: 13 Outlet Region's of the Greenland Ice Sheet. Grouping the outlet regions first by Sector and then the actual latitude and longitude is given. See Figure 1.1. This is where the initial positions are distributed homogeneously in the model grid.

Sector	Outlet Region Name	Range (Latitude)	Range (Longitude)
North	Petermann Glacier (PG)	81.1418 : 81.3186	-63.1194 : -61.3583
North West	Kong Oscar to Illullip Sermia (KO2I)	74.3360 : 76.0181	-56.5508 : -59.9248
Centre West	North of Sullorsuaq (NSULL)	70.7310 : 71.5803	-53.9087 : -54.6281
Centre West	Sullorsuaq (SULL)	70.1871 : 70.3047	-53.0833 : -53.2168
Centre West	Disko Bay (DB)	68.4373 : 69.5542	-52.5816 : -52.8834
South West	Nuuk (NU)	63.6618 : 64.2716	-51.4033 : -51.9598
South West	Julianehab (JUL)	60.4027 : 60.6756	-46.3048 : -47.9175
South East	Helheim Glacier (HEL)	65.2663 : 65.5468	-37.3970 : -39.8287
Centre East	Kangerdlugssuaq Glacier (KGLQ)	67.8649 : 68.1845	-31.1852 : -32.4753
Centre East	Kong Christian IV Glacier (KCIV)	67.9325 : 68.2284	-29.4785 : -30.1129
Centre East	Scoresby Sund (SBS)	70.0942 : 70.4951	-20.9884 : -22.8677
North East	Zachariae Isstrom (ZI)	78.7014 : 79.1333	-20.1541 : -20.9219
North East	Nioghalvfjerdsfjorden (79NG)	79.3690 : 79.6678	-21.0201 : -21.4409

Table 2.4: Experiments using the ANHA-NEMO Configuration

Simulation		Integration	Sea Ice Model	Initial Condition	Open Boundary Conditions	Atmospheric Forcing	Runoff	Output
ANHA12 Reference	ANHA12-EXH003	2002-2010	LIM2	GLORYS1v1	GLORYS1v1[a]	CGRF[b]	monthly climatology (on-the-fly)	5-day NORMAL
ANHA4 Reference	ANHA4-E34REF	2002-2010	LIM2	GLORYS1v1	GLORYS1v1[a]	CGRF[b]	monthly climatology (on-the-fly)	5-day NORMAL
ANHA4 Runoff Remap-II	ANHA4-TEST12	2002-2010	LIM2	GLORYS1v1	GLORYS1v1[a]	CGRF[c]	monthly climatology with Greenland melt (remap-II)	5-day NORMAL

[a]Switched to GLORYS2 after 2008

[b]Solid precipitation (snow) taken from inter-annual CORE-II

[c]Solid precipitation (snow) computed from CGRF total precipitation based on the 2-m air temperature

Chapter 3

Ocean Circulation and Marine Terminating Glaciers of the Greenland Ice Sheet

3.1 Abstract

Higher latitudes have experienced a significant change in climate and physical processes within recent years. This study focuses on the Greenland Ice Sheet and surrounding ocean waters. It has been shown that relatively warm ocean waters may accelerate melt production of marine terminating glaciers. We explore and classify the pathways for the warmer Atlantic waters that reach the fjords along the coasts of Greenland. Additionally, given that the melt of these glaciers is accelerating, we look at the pathways of the low salinity melt waters from these coastal glaciers and where it is taken up in the surrounding basins. This analysis was carried out using Arctic and North Hemisphere Atlantic (ANHA) configurations of the Nucleus for European Modelling of the Ocean (NEMO) ocean/sea-ice general circulation model run at both $\frac{1}{4}^o$ and $\frac{1}{12}^o$ resolution. Pathways were determined using the ARIANE Lagrangian float package using both forward and backward trajectories. Warm waters that reached the north and west coast of Greenland tended to be fed by

the relatively warm and saline Irminger Current. The south east and the east Greenland coast tended to have warm waters advected to them through Nordic Seas.

3.2 Introduction

The Greenland Ice Sheet's mass loss has accelerated over recent years (Box *et al.*, 2006; Rignot & Kanagaratnam, 2006; Van Den Broeke *et al.*, 2009; Shepherd *et al.*, 2012) with the freshwater anomaly, since 1995, reaching around $\frac{1}{3}$ of the amount of the 1970s Great Salinity Anomaly (Bamber *et al.*, 2012). Within a 20 year period the mass balance estimates have quadrupled from -51 +/- 65 Gt/year during 1992 to 2000, to -211 +/- 37 Gt/year during 2000 to 2011 (Shepherd *et al.*, 2012) and melting period had also lengthened (Box *et al.*, 2006). The GrIS contributed 6.1 mm/decade of sea level rise from the period of 2002 to 2010 (Fichefet *et al.*, 2003).

Suggested causes of mass loss from the GrIS include: increased surface air temperatures (Rignot & Kanagaratnam, 2006; Hanna *et al.*, 2013; Straneo & Heimbach, 2013), the positive feedback from the decrease in Arctic sea ice impacting polar temperatures (Hanna *et al.*, 2013), warmer ocean temperatures around Greenland (Rignot & Kanagaratnam, 2006; Holland *et al.*, 2008; Myers & Ribergaard, 2013; Straneo & Heimbach, 2013; Jackson *et al.*, 2014), and the fluctuation of heat content in the North Atlantic Subpolar Gyre (NASPG) (Myers & Ribergaard, 2013; Holland *et al.*, 2008). In non summer months, atmosphere temperatures are low and therefore glacial melt has a large dependency on the externally forced ocean exchange onto the Greenland shelf towards the ice sheet's glaciers (Jackson *et al.*, 2014).

The North Atlantic Current (NAC) forms the southern part of

the NASPG (Figure 1.1). The Irminger Current is formed when part of the NAC separates and circulates along the Reykjanes Ridge (Fratantoni & Pickart, 2007). The Irminger Current typically travels along southeast Greenland where it merges with the East Greenland Current (EGC), rounding Cape Farewell and subducting under the low-salinity polar water, forming the West Greenland Current (WGC) (Straneo, 2006; Fratantoni & Pickart, 2007; Melling *et al.*, 2008; Myers *et al.*, 2009). Along Greenland's eastern shelf, the East Greenland Coastal Current (EGCC) travels past Cape Farewell, carrying very fresh polar waters, as well as Greenland melt (Bacon *et al.*, 2014).

The WGC separates into two branches: one travels northward along the west coast of Greenland into Baffin Bay, bringing with it both less saline, cold Polar water and relatively warm, saline, modified Irminger Sea water (Myers *et al.*, 2009) and the second, warmer and more saline branch joins the southward flowing Baffin Island Current at Davis Strait (Fratantoni & Pickart, 2007).

It is the heat content available from the Irminger Current and EGC that may influence the total freshwater flux (FWF) of a marine terminating glacier on the GrIS (Holland *et al.*, 2008; Straneo *et al.*, 2012; Straneo & Heimbach, 2013; Myers & Ribergaard, 2013). The warmest Atlantic water near the GrIS is found near the southeast and then the northwest and central-west sectors of Greenland (Straneo & Heimbach, 2013; Straneo *et al.*, 2012). The northern sectors of the GrIS are bounded by cool polar waters and oceanic heat may not play an important role in that region of GrIS (Straneo & Heimbach, 2013; Straneo *et al.*, 2012). The northwest and southeast sectors of GrIS account for 80% of the ice sheet's discharge (Enderlin *et al.*, 2014). Both regions have experienced the largest increase in total FWF from the 1990s to 2010 (Bamber *et al.*, 2012), a time

when NASPG waters were a record high due to the slow down of the gyre (Straneo & Heimbach, 2013).

There has been an increased presence of warmer waters in fjords of fast-moving marine terminating glaciers such as Jakobshavn in Disko Bay (Holland *et al.*, 2008; Myers & Ribergaard, 2013), and south east glaciers, Helheim (Sermilk Fjord) and Kangerdlugssuaq (Kangerdlugssuaq Fjord) (Christoffersen *et al.*, 2011; Sutherland *et al.*, 2014), which occurred at the time these marine terminating glaciers retreated (Holland *et al.*, 2008; Myers & Ribergaard, 2013; Christoffersen *et al.*, 2011).

The west branch of Baffin Bay circulates cold waters southwards through Davis Strait, accompanied by the outflow through Hudson Strait (Fratantoni & Pickart, 2007), into the Labrador Current, where freshwater may circulate in to the Labrador Sea (connected to the west of the NASPG, defined by the 3300 metre isobath (Straneo, 2006)) (Melling *et al.*, 2008). There are many sources of freshwater that enters the NASPG: river runoff, waters from the Arctic Ocean through the Canadian Arctic Archipelago (CAA) and Hudson Strait, sea ice, icebergs, and the GrIS being the largest reservoir for freshwater (Dickson *et al.*, 2007).

The Labrador Sea has significant biological activity, intense air-sea interactions, extreme winds, cold temperatures, icebergs and sea ice (Marshall *et al.*, 1998). Buoyancy-driven convection occurs in the Labrador Sea (Myers *et al.*, 2009). This deep water formation links to the North Atlantic Deep Water (NADW) current (Weijer *et al.*, 2012). Buoyancy-driven convection may be sensitive to heat loss and freshwater input in the central Labrador Sea, as one will drive deep convection and the other, lower the density of the surface waters, slowing down convection (Aagaard & Carmack, 1989; Straneo, 2006; Weijer *et al.*, 2012).

The NADW makes the deep branch of the Atlantic Meridonal Overturning Circulation (AMOC), therefore changes in the rate of convection at the Labrador Sea may have an impact on the AMOC (Dickson *et al.*, 2007; Weijer *et al.*, 2012). The AMOC is responsible for northward heat transport in the upper ocean waters, and deep southward flow of cold water, and therefore has a strong influence for our climate system (Dickson *et al.*, 2007; Weijer *et al.*, 2012).

In recent years, there has been discussions on how GrIS enhanced melt may affect ocean circulation (Fichefet *et al.*, 2003; Swingedouw *et al.*, 2014). Where the freshwater is released and how it is taken up by the oceanic circulation surrounding Greenland may have different implications on other systems. The sensitivity of the AMOC to FWF varies depending on different climate model simulations, though they come to the same result, with increased FWF from the GrIS the AMOC will go undergo a weakening phase (Fichefet *et al.*, 2003; Swingedouw *et al.*, 2014). A slowdown of this circulation and its heat transport could have a significant impact on how the earth regulates its temperatures (Straneo & Heimbach, 2013).

3.3 Methods

We used a primitive equation, eddy permitting, system of numerical models, Nucleus for European Modelling of the Ocean (NEMO) version 3.4, to examine pathways of GrIS melt, as well as source the warm waters found near marine terminating glaciers. To represent sea ice, NEMO is interfaced with a sea ice thermodynamic and dynamic numerical model, the Louvain la-neauve Ice Model (LIM2) (Fichefet & Morales Maqueda, 1997; Madec, 2008). The ocean engine, Ocean Parallelise (OPA), is used for ocean dynamics and thermodynamics on a three dimensional Arakawa C-type

staggered grid. We compared 3 different experiments with a regional Arctic Northern Hemisphere Atlantic (ANHA) configuration: a $1/4^o$, ANHA4 reference run and ANHA4 with additional runoff (Dukhovskoy *et al.*, submitted) and $1/12^o$ ANHA12, hereinafter called ANHA4REF, ANHA4RUNOFF and ANHA12, respectively.

The domain of the high-resolution output from the ANHA configuration covers the whole Arctic Ocean, North Atlantic and part of South Atlantic, with two open boundaries: one at Bering Strait and the other at 20^oS (Dukhovskoy *et al.*, submitted). The configuration's mesh grid is extracted from a global configuration on a tripolar grid, ORCA (DRAKKAR *et al.*, 2007).

Initial conditions were provided by Global Ocean Reanalyses and Simulations (GLORYS1v1) which include: temperature, salinity, sea surface height and horizontal velocities (zonal and meridonal) as well as monthly open boundary conditions for the same fields (Ferry *et al.*, 2008). The reanalysis forecast error covariance, used in GLORYS, is based on statistics of a collection of 3 dimensional ocean state anomalies with seasonal variability (Ferry *et al.*, 2008). The ocean initial condition in temperature and salinity is based on ARIVO global climatology with the first three months considered as a spin-up of GLORYS-1 system (Ferry *et al.*, 2008). The initial ice field is a combination of ice concentration and ice thickness (provided by satellite observation and GLORYS1v1 respectively). The LIM2 ice model assumes that ice behaves as an elastic viscous plastic dynamical system to include the interaction of the stress between ocean and ice computed at each time step (Fichefet & Morales Maqueda, 1997; Ferry *et al.*, 2008).

Fields were taken from GLORYS1 (2002 to 2007) and GLORYS2 (2008-2010) in the ANHA configuration (Ferry *et al.*, 2012). For the ANHA configuration, the atmospheric forcing data, provided by

Canadian Meteorological Centre's (CMC) global deterministic prediction system (GDPS) reforcasts (CGRF) dataset (Smith *et al.*, 2014) has hourly 33km resolution for the following fields: 10 metre surface wind, 2 metre air temperature and humidity, downward shortwave and longwave radiation and total precipitation. From the total precipitation, snowfall is represented when temperature at the surface is greater than 0^oC, and rain otherwise (Hu, 2015, personal communication). Snowfall is provided by the inter-annual Coordinated Ocean Research Experiments (CORE) v2 dataset (Large & Yeager, 2008).

The experiments used here have been structured and set up by Paul Myers' Geophysical Fluid Dynamics Ocean Modelling Group at the University of Alberta in the Earth and Atmospheric Sciences Department
(http://knossos.eas.ualberta.ca/xianmin/anha). Full details on the configuration is listed in Table 2.4. All of the reference experiments (ANHA4REF and ANHA12) include the total runoff into regions on the ocean grid by direct interpolation (on the fly) by NEMO's bilinear interpolation of Dai and Trenberth $1^o \times 1^o$ gridded monthly climatology. The ANHA4RUNOFF experiment includes the Greenland meltwater (Bamber *et al.*, 2012) (a volume conserving, resolution independent, directionally distributed runoff data field) applied onto the ocean model grid (Remap-II) (Dukhovskoy *et al.*, submitted).

1. ANHA4REF ANHA at $\frac{1}{4}^o$ horizontal grid framework comes from ORCA025 (DRAKKAR *et al.*, 2007), resolution ranges from ∼5.79km in northern Canada and ∼27.9km at the equator. Runoff data is interpolated from a $1^o \times 1^o$ global monthly climatology dataset (Dai *et al.*, 2009). See Figure 2.2.

2. ANHA4RUNOFF

   Is the same set up as ANHA4REF except runoff is monthly climatology with Greenland melt (Bamber *et al.*, 2012) (remap-II) (Dukhovskoy *et al.*, submitted). This method provides more accurate runoff input to reduce the salinity drift in the experiment. See Figure 2.2.

3. ANHA12

   The $\frac{1}{12}^{o}$ horizontal resolution, has a resolution of ∼1.93km near the artificial pole over northern Canada and ∼9.3km at the equator. Runoff data is interpolated from a $1^{o} \times 1^{o}$ global monthly climatology dataset (Dai *et al.*, 2009). See Figure 2.3.

The offline Lagrangian tool that uses model output velocity fields as an input, ARIANE (Blanke & Raynaud, 1997), is used on our NEMO simulation. ARIANE's diagnostics are based on the calculation of multiple trajectories to integrate particle trajectories in the three dimensional modelled velocity field (Blanke & Raynaud, 1997). Calculations are with time, moving forwards or backward, fitted to the nature of the ocean circulation (Blanke & Raynaud, 1997). This method for computing a trajectory is fast and accurate as it only calculates positions on the edge of individual grid cells, offline, not having to be run with the model (Blanke & Grima, 2008).

ARIANE has a namelist that checks the particularities of the model grid that is read. We have set ARIANE to not read all the data at once by setting a sequential parameter, therefore the interpolation is done in space (Blanke & Grima, 2008). ARIANE has the option to run a qualitative or quantitative experiments (Blanke & Grima, 2008). In our study we ran the former to fully monitor the successive positions, where quantitative would evaluate the mass

transport between the initial and final location (Blanke & Grima, 2008). We set ARIANE to account for the partial cell depths as well as vertical integration of the divergence from the horizontal movement. By default ARIANE applies an upward integration from the flow of the ocean bottom (vertical velocity equals zero) to the surface (Blanke & Grima, 2008). The integration of vertical velocity can cause an error at the surface of nonzero values, such that particles will enter the atmosphere.

ARIANE also allows backward integration, which can be performed to track the origin of a given region of water (Blanke & Grima, 2008). ARIANE provides an estimate of transport with particles whose initial positions are homogeneously distributed in space and time (Blanke & Grima, 2008). Particles evolve based on the Eulerian output fields (temperature, density and salinity), however certain process cannot be resolved from the Lagrangian calculations, e.g. diffusion and convective mixing. The Eulerian output fields from the ocean model include the parameterization of such processes in the ocean tracer and dynamic fields. Therefore, ARIANE should produce a reliable representation of tracer movement.

Backwards integration for the same 13 outlet regions (Table 2.3) was done to find each location's warm water source by releasing 5000 particles throughout the entire water column. We examined a specific water mass where temperature and salinity are that of the warm water sourced from the Irminger Sea. See Table 2.2 for definitions of temperature and salinity per region. Each region required an individual analysis to search for the water mass that was relatively saline with temperatures greater than 0^{o}C. When possible, the salinity criteria was increased to capture the most saline and relatively warm, water mass.

To simulate how the surface waters at each outlet region get taken up by the surrounding ocean currents, about 1000 initial positions were initialized in the first 21 model grid level of the water column (77.85 metres) and then the Lagrangian calculations done by the ARIANE offline tracking tool over a 5 model year run by moving forward in time.

To analyze our results, we have two separate tasks; backwards integration and forward integration from our outlet regions. The analysis was done using the output (5 day) velocity fields for years 2002-2010 for ANHA4 and ANHA12 for each outlet region to examine the pathways and how they evolved through the forward and backward integration.

We examined the pathways the virtual float followed in our horizontal grid. To set a probability, the total occurrences in a grid cell is divided by the total occurrences for a float in all grid cells for of all years. ARIANE was initiated at a specific time with initial positions set by our 13 outlet regions (Table 2.3) and the tracers recorded the positions along their trajectories for 5 years. For our forward calculations, the start time for all experiments is the beginning of each year (e.g. January 5th, 2002, January 5th, 2003, January 5th, 2004, January 5th, 2005, January, 5th 2006), and then run for 5 years forward in time. For the backward calculations, the initial start time for all experiments was at the end of each year (e.g. December 30th, 2010, December 30th, 2009, December 30th, 2008, December 30th, 2007, December 30th, 2006) and then run for 5 years backwards in time.

We plotted the 5 year average for all 13 locations, backward and forward integration. Results showed the likelihood that a particle was contained in a grid cell in our configuration. This was done by looking at the total number of particles throughout the 5 year

offline run, and how many times a particle entered the grid cell. From the calculated values, we got a quantitative measurement of warm water sources and thus how the freshwater content may be taken up into the ocean.

Probability terms are defined in Table 2.1. These values correspond to the percentage that out of all floats and grid cells, the percentage that one parcel (as defined by the specific parameter of temperature and salinity) was contained in that grid during the 5 year simulation.

3.4 Results

See Table 3.1, for the definitions used to define specific depths.

For the forward trajectory analysis, outlet regions close in proximity to one another had slight differences in results. This is why I have grouped the outlet regions together for the forward analysis. I've kept each region separate for the Backward trajectory analysis as each region seemed to have a unique solution with changing water mass definition per region (See Table 2.2).

3.4.1 Origin of Warm Water

Petermann Glacier (PG)

Warm water in the outlet region of Petermann Glacier (PG) (Figure 3.1 and 3.2 (1.a,b,c)) is defined as a water mass with a temperature greater than 0.2^{o}C and salinity higher than 34.1 g/kg. The backward trajectories have shown that PG received warm water from the north end of Nares Strait at subsurface depth. These warm waters could have come from two pathways. One was originally from the Lincoln Sea Shelf with high to medium probability and the other one from the surface water on north Greenland Shelf

with medium to low probability. The two paths were consistent in all the three configurations, however, ANHA12 showed these warm waters could be tracked back much further, off the East Siberian Shelf. There was a low to very low probability of these waters originated from the interior of the Arctic Ocean, following the basin boundary clockwise and then along the transpolar current.

Kong Oscar to Illullip Sermia (KO21)

Moving to the section of the coast from Kong Oscar to Illullip Sermia (KO2I) (Figure 3.1 and 3.2 (2.a)), located in the northwest of Baffin Bay, warm waters (T>0.2^{o}C, S>34.1 g/kg) were found to have very high to high probability of coming from the west Greenland shelf at subsurface depths. At the same time, there was medium to high probability tracks of waters from Baffin Bay interior were observed, ranging from sub-intermediate to deep depths. There was medium to low probability of tracks came from the subsurface to deep depths in the NAC and then travelled around the south east of Greenland. It was also possible to have warm waters come through the CAA via Lomonsov Ridge, as well as from the Greenland Sea, although the probability was low to very low from the last pathway. This section might have shown the impact of resolution, as these warm waters were only observed in the higher resolution configuration (ANHA12) and not at lower resolutions (ANHA4REF and ANHA4RUNOFF).

North of Sullorsuaq (NSULL)

Moving further south in Baffin Bay, warm waters (T> 0.2^{o}C, S> 34.1 g/kg) at the mouth of the bay north of Sullorsuaq (NSULL) (Figure 3.1 and 3.2 (3.a,b,c)), were tracked back to surface and subsurface waters came from the west, the south west and the south

east Greenland shelf, all with high probabilities. Floats reached with medium probability: sub-intermediate and deep interior Baffin Bay waters, intermediate to sub-intermediate waters came from the EGC, subsurface to sub-intermediate waters from Greenland sea, and intermediate waters from Irminger sea and surface to sub-intermediate waters came from the NAC. Warm origin of source waters potentially triggering the melting of glaciers.

ANHA12 tracked waters with medium probability to come from the CAA at surface to subsurface depths, while ANHA4 configuration tracked waters with medium probability came from the Labrador Current and around the subpolar gyre.

Sullorsuaq (SULL)

Sullorsuaq (SULL) (Figure 3.1 and 3.2 (4.a)), represented only in AHA12 due to the resolution. Therefore in this section, all findings were based on the ANHA12 simulation only. Warm waters were defined here as temperature greater than 0.2 ^{o}C and salinity greater than 34.5g/kg.

Backward trajectories have shown the highest probabilities on the west Greenland shelf (depths of surface to subsurface), as well as around Disko Bay (DB) (discussed in further details later). Intermediate to sub-intermediate waters reach this region from the interior Baffin Bay. Surface to subsurface waters from CAA and Nares Strait as well as intermediate to sub-intermediate depths from EGC and surface to sub-intermediate waters from Greenland Sea. Subsurface to sub-intermediate waters from Irminger Sea and NAC could reach SULL with medium probability. Low probability of waters came from the Arctic Ocean, Chukchi Shelf across the Lomonsov Ridge, interior Labrador Sea and Labrador Current.

Disko Bay (DB)

In DB (Figure 3.1 and 3.2 (5.a,b,c)), all the three simulations have shown that warm water (T>0.2^{o}C, S>34.5 g/kg) could be tracked in the surface and subsurface waters of WGC, then the intermediate waters from the Irminger Current and Irminger Sea and finally the surface to intermediate depths of the NAC. However, ANHA4 simulations have shown relatively higher probability in the NAC, particularly in the ANHA4RUNOFF simulation. The ANHA4 simulations have shown that waters from the Labrador Current reached DB. This means waters might join the NAC at the Grand Banks, although the probability was low. The probability was lower(very low) with the higher resolution simulation ANHA12 Figure 3.1(5.a). Another route revealed by the trajectories was that warm waters from the EGC and Greenland sea also reach DB, with medium probability. ANHA12 and ANHA4REF have shown depths of intermediate to sub-intermediate while ANHA4RUN showed surface to intermediate depths. This path flows down to the south via Denmark Strait and then around the southern tip of Greenland.

There was also a medium probability that waters come from the interior of Baffin Bay. ANHA12 and ANHA4REF have shown that waters of subsurface to sub-intermediate depths and ANHA4 have shown that waters from subsurface depths. ANHA12 have shown that a medium probability that these waters were fed at surface to subsurface depths from the CAA and Nares Strait.

Nuuk (NU)

Warm water (T>0.2^{o}C, S>34.7 g/kg) found near the outlet region of Nuuk (NU) (Figure 3.1 and 3.2 (6.a,b,c)), could be tracked with high probability in subsurface to intermediate layers, but along

the WGC and Irminger Currents. These waters in the EGC, Greenland Sea, and Irminger Sea were found at depths of surface to sub-intermediate (ANHA12) or surface to intermediate (both ANHA4 configurations). With a medium probability, some of these waters could be tracked both to Fram Strait and the Nordic Seas at depths of surface to sub-intermediate (ANHA12) or surface to intermediate (both ANHA4 configurations). Going farther back along the pathways there was a medium probability that waters could be tracked to the NAC at surface to sub-intermediate depths. The ANHA4 configurations found waters came all the way from the Labrador Current and Davis Strait with medium probability at depths of surface to subsurface. However ANHA12 found this source to be of low to very low probability. Similar low probabilities exist for the Eurasian Basin in the Arctic Ocean.

Julianehab (JUL)

Warm water (T>0.2^{o}C, S>34.88 g/kg) found by the outlet region near Julianehab (JUL) (Figure 3.1 and 3.2 (7.a,b,c)), could be tracked with both high probability in the surface to sub-intermediate waters of the EGC. ANHA12 found waters from surface to intermediate came from the Greenland Sea with high probability. ANHA12 have shown that high probability of water came from the Irminger Current in the surface to subsurface, while the ANHA4 configurations have shown surface to sub-intermediate depths. There was a medium probability for water to come via the the route of Fram Strait, Nordic Sea and NAC, at depths ranging from surface to sub-intermediate. The ANHA4 configurations found medium probability for water at the surface and subsurface to come from Davis Strait and the Labrador Current, while ANHA12 had a low to very low probability.

Helheim Glacier (HEL)

Compared to other glaciers on the west side of Greenland, as is discussed previously, the region offshore of Helheim Glacier's (HG) outlet receives very little warm water (T>0.2^{o}C, S>34.88 g/kg) of Irminger Sea origin (Figure 3.1 and 3.2 (8.a,b,c)). All simulations do show high probability of warm water being transported by the EGC south through Davis Strait.

The dominate portion of the warm water comes from the west Nordic Seas (Iceland Sea and Greenland Sea). Both ANHA12 and ANHA4REF found the waters at depths ranging from surface to subsurface, while in ANHA4RUNOFF they came deeper from the surface to the intermediate depths. With medium probability, the warm water could then be tracked back to the NAC at depths of surface to sub-intermediate. This was associated with flows north into the Nordic Sea through the Iceland-Scotland Ridge. These waters then circulate counterclockwise with medium probability at surface to sub-intermediate (ANHA12,ANHA4REF) or surface to intermediate depths (ANHA4RUNOFF).

I also observe a medium probability, at surface to sub-intermediate depths, in ANHA12 and to deep depths in the ANHA4 runs, of re-circulated Atlantic Water north of Fram Strait (could extend to Eurasian Basin with low to very low probability in ANHA12).

ANHA4RUNOFF have shown that the Labrador Current and Davis Strait waters to have medium probability of reached this glacier at depths of surface to subsurface. The higher probability shown in ANHA4RUNOFF indicates that the amount of runoff does play a role in the flow through Davis Strait, and along the Labrador Sea shelf.

Kangerdlugssuaq (KGLQ) and Kong Christian IV (KCIV)

These two regions have similar results due to their proximity. Warm water(T>0.2^{o}C, S>34.1 g/kg) found by the outlet region of Kangerdlugssuaq (KGLQ)(Figure 3.1 and 3.2 (9.a,b,c)) and Kong Christian IV (KCIV) glaciers (Figure 3.1 and 3.2 (10.a,b,c)) could be tracked with very high probability in the ANHA4RUNOFF configuration at surface and subsurface depths to waters recirculating nearby on the east Greenland shelf. There were high probabilities of this region being fed by the east Greenland Shelf, EGC, and the Greenland Sea at depths of surface to sub-intermediate (ANHA12 and ANHA4RUNOFF) or surface to subsurface (ANHA4REF). Note that ANHA4REF found the warm waters at shallow depths,
ANHA4REF did show a medium probability of floats came from Voring and Faroe Plateaus at intermediate depths, similar to the other configurations. There was a medium probability that floats would come through Fram Strait at surface to deep depths. In the Nordic Sea, the warm water was found at depths of surface to sub-intermediate (ANHA12 and ANHA4RUNOFF), or surface to subsurface (ANHA4REF). There was a medium probability of water came from the NAC at depths from surface to intermediate.

Scoresby Sund (SBS)

Warm water (T>0.2^{o}C, S>34.7 g/kg) was found by the outlet region of Scoresby Sund (SBS) (Figure 3.1 and 3.2 (11.a,b,c)) could be tracked with very high probability to water at surface to subsurface depths on the East Greenland Shelf. There was a medium to high probability of this water previously came through Fram Strait at intermediate and deep depths. ANHA12 and ANHA4REF found this water at similar depths in the EGC, where ANHA4RUNOFF

found this water at intermediate and sub-intermediate depths. Further back, we see medium probabilities in the Nordic Seas at subsurface to intermediate depths. There were only low to very low probability of floats came from the NAC and south of Denmark Strait that could reach this glacier. The high probabilities north of Greenland indicates that re-circulated Atlantic water that flows into Arctic Ocean through Fram Strait might not be the only source of Atlantic water that reaches SBS. ANHA12 have shown that more warm water from Iceland Sea but this was not seen in the ANHA4 simulations.

3.4.2 Pathway of Fresh Meltwater

North Greenland: Petermann Glacier (PG)

Surface waters found by the outlet region of PG (Figures 3.3 and 3.4 (1.a,b,c)) have a high probability to head south through Nares Strait at surface and subsurface depths and enter Baffin Bay interior reached sub-intermediate depths. This pathway does not extend to the west Greenland shelf. There was a high to medium probability that waters would continue south, at surface to subsurface depths, through Davis Strait. They then continue south along the Labrador Current into Flemish Pass, and west onto the Scotian Shelf. There was a medium probability of floats entering the NAC at surface to deep depths, reached the Iceland Basin to surface and subsurface depths.

North West Greenland: Kong Oscar to Illullip Sermia (KO2I), North of Sullorsuaq (NSULL), Sullorsuaq (SULL)

Compared to meltwater from PG, surface waters released in this region: KO2I(Figures 3.3 and 3.4 (2.a)), NSULL (Figures 3.3 and 3.4 (3.a,b,c)), and SULL (Figures 3.3 and 3.4 (4.a)), had a very high

probability of recirculating on the west Greenland shelf at surface to subsurface depths. There was then a high probability of waters entering eastern Baffin Bay at surface to subsurface depths, and travelled south through Davis Strait into the Labrador Current to Flemish Pass and onto Scotian Shelf. Water from NSULL and SULL reach deep depths off the Canadian shelf.

There was a medium probability that waters would recirculate in Baffin Bay reached intermediate and sub-intermediate depths. There was also a medium probability that floats would be entrained in the NAC. These waters subduct into deep depths off of the Canadian Shelf and then rise up in the water column to subsurface levels as they travel across the Atlantic Ocean.

North West - South West Greenland: Disko Bay (DB), Nuuk (NU), Julianehab (JUL)

Surface waters found by the outlet regions of DB (Figures 3.3 and 3.4 (5.a,b,c)), NU (Figures 3.3 and 3.4 (6.a,b,c)) and JUL (Figures 3.3 and 3.4 (7.a,b,c)) have a high probability of recirculation in surface to subsurface depths in Baffin Bay. There was a high probability that these waters remain along west Greenland shelf at surface and subsurface depths. There was also a high probability that they enter Baffin Bay at deep depths. As well the probability was high of waters entering Davis Strait at surface to subsurface, flowing into the Labrador Current, where they subduct off the Canadian Shelf into deep depths near the Scotian Shelf. There was a medium probability that these waters would enter the NAC, shoaling to surface and subsurface depths as they head east across the Atlantic Ocean. Medium probabilities continue as these waters entered the eastern subpolar gyre, in the Irminger Current intermediate to sub-intermediate depths, Some of these waters passed the southern tip

of Greenland into the Labrador Sea at deep depths. There was a low to very low probability that these waters would enter the interior subpolar gyre and the Nordic Seas. Waters originating in JUL, farther south, were more likely to be found deeper in the water column. ANHA12 has less exchange across the Atlantic Ocean and into the interior subpolar gyre circulation, with the floats being more constrained to the coast.

South East Greenland: Helheim Glacier (HEL)

Surface waters from outside the fjord near HG (Figures 3.3 and 3.4 (8.a,b,c)) would flow west past the southern tip of Greenland, initially at surface to subsurface depths before descending. ANHA12 has a high probability of these water entering Davis Strait at surface to intermediate depths. There was also a high probability of water entering the Labrador Current, and flowing to the Scotian Shelf, at surface and subsurface depths. ANHA12 found a medium probability of waters entering WGC at surface to subsurface intermediate depths. All configurations have shown waters entering Baffin Bay at sub-intermediate to deep depths with the highest probability in ANHA12. There was a medium probability of these waters entering the Labrador Sea interior, off the shelf, and then into the NAC.

South East - North East Greenland: Kangerdlugssuaq (KGLQ), Kong Christian IV (KCIV), Scoresby Sund (SBS)

Surface waters found by outlet regions of KGLQ (Figures 3.3 and 3.4 (9.a,b,c)), KCIV (Figures 3.3 and 3.4 (10.a,b,c)) and SBS (Figures 3.3 and 3.4 (11.a,b,c)) have a very high probability of recirculating locally at surface to subsurface depths. There was a high probability of waters entering the WGC. There was very little exchange back into the Irminger Sea. There was a high probability of

these waters entering Davis Strait at subsurface to sub-intermediate depths, as well as entering the Labrador Current at intermediate to deep depths. There was a medium probability of these waters being found at sub-intermediate to deep depths in Baffin Bay, deep depths in the Labrador Sea interior, as well as along the NAC. There was a medium probability that these waters would enter the Nordic Seas in the Ice land Irminger Current.

North East Greenland: Zachariae Isstrom (ZI) and Nioghalvfjerdsfjorden (79NG)

Surface waters found by outlet regions of Zachariae Isstrom (ZI) (Figures 3.3 and 3.4 (12.a,b,c)) and Nioghalvfjerdsfjorden (79NG) (Figures 3.3 and 3.4 (13.a,b,c)), have a very high probability of recirculating close to the outlet region at surface to subsurface depths. There was a high probability of these waters reached the west Greenland shelf at surface to subsurface depths. There was a medium probability of this water would enter the WGC. There was a medium probability of this water entering sub-intermediate to deep depths in Davis Strait, subsurface to deep layers in Baffin Bay and offshore branch of the Labrador Current deep depths. There was a medium probability that such melt waters would travel north of Greenland through Fram Strait at surface to subsurface depths. This pathway then flows into Nares Strait at surface to intermediate depths.

3.5 Discussion and Conclusions

Our study has shown that freshwater from north and northwest and southwest Greenland would mix into Baffin Bay by transportation through the WGC, as seen in previous studies with coarser resolution (Marsh *et al.*, 2010; Castro de la Guardia *et al.*, 2015). At

the southeast regions, including SBS, the freshwater travelled along the EGC and WGC and has a low likelihood of entering Baffin Bay, instead being directly transported south via Davis Strait into the Labrador Current, which agrees with studies done in Dukhovskoy et al., (in press), showing Greenland freshwater propagating through sub-Arctic seas. Therefore our work alludes to the theory that the high export of freshwater from northwest GrIS (second highest freshwater export on the GrIS (Bamber *et al.*, 2012)) has a higher likelihood of impacting Baffin Bay than all other regions of the GrIS. This freshwater input into Baffin Bay may alter the circulation patterns in Baffin Bay and increase the sea surface height (Marsh *et al.*, 2010; Castro de la Guardia *et al.*, 2015), which may play a role in the future transport of Arctic waters passing through the CAA.

The highest freshwater export from the GrIS (southeast section (Bamber *et al.*, 2012)) will have larger implications for circulation in the NASPG. This export of freshwater will not be as likely to be taken into Baffin Bay, which was not the case in the modelled runoff experiments (with coarser resolution) in Castro de la Guardia (2015). The different results could be from the coarser resolution not being able to resolve mixing from the WGC into the Labrador Sea, as well as different model forcing.

The tracks made from the freshwater paths showed this freshwater from southeast GrIS getting entrained into depths greater than 1000 metres in the interior of the Labrador Sea. Previous studies have analyzed the impact that an increase in freshwater in the interior of the Labrador Sea may reduce the Atlantic Meridonal Overturning Circulation (AMOC) (Belkin *et al.*, 1998; Swingedouw *et al.*, 2006; Myers & Donnelly, 2008; Marsh *et al.*, 2010; Gelderloos *et al.*, 2012; Weijer *et al.*, 2012; Swingedouw *et al.*, 2014).

An anomalous event where surface waters increased in buoyancy (in 1968) led to winter convection, shutting down for the next 3 years,the 1970s GSA (Gelderloos *et al.*, 2012). Our study contributes to the theory and observations as the GrIS continues to melt (as the freshwater anomaly, since 1995, has reached around $\frac{1}{3}$ of the amount of the 1970s GSA (Bamber *et al.*, 2012)), it will have an impact on the AMOC, and has the potential to cause a complete shut down, especially with mild winters which was observed in the 1970s case.(Gelderloos *et al.*, 2012). Freshwater from further northeast (ZI, 79NG) is contained to the East Greenland Coastal Current along the shelf north of Cape Farewell.

Our study agrees with previous observations and models, that warm water comes in close proximity to the northwest coast (Holland *et al.*, 2008; Straneo *et al.*, 2012; Myers & Ribergaard, 2013) and to the south and south east coast of the GrIS (Straneo *et al.*, 2012; Straneo & Heimbach, 2013; Inall *et al.*, 2014; Jackson *et al.*, 2014). Our study takes this one step further and found where the warm waters originated. Warm water came in contact with PG and KO21 were made up of Arctic and CAA waters, where Straneo (2012) found PG to have the coldest warm Atlantic water. Further south at NSULL, SULL and DB, warmer waters came from Baffin Bay and the Irminger Sea. The Greenland and Nordic Seas become a source of warm waters for the southern coast of Greenland (NU, JUL, HEL) which were also received warm waters directly from the Irminger Sea via Irminger Current. The Greenland Sea and Nordic Sea become the sole contributor for the transport of warm waters to the east part of Greenland (KGLQ, KCIV, SBS). Straneo (2010) found the warmest Atlantic Water was found by HEL and DB, while we found HEL had two sources of warm water (Greenland/Nordic Sea and Irminger Sea) and DB had Baffin Bay and the Irminger

Current. Therefore sections with warm water origins from both the Irminger Current and Greenland/Nordic Seas may have the highest heat content.

The next in Straneo's (2010) study to have the warmest Atlantic Water was KGLQ (which we found is fed from the Greenland and Nordic Seas) and then 79NG, where our experiments could not pick up warm waters along the north east portion of Greenland (ZI, 79NG). Comparing with observations (Rhein, personal communication, September 6th, 2015), observations have shown warm waters reaching 79NG. Therefore, we need to further examine the complex circulation along the east Greenland Shelf to compare the varying results.

Oceanic heat may not be playing a large role in the northeast sector of the GrIS (where our experiments could not resolve warm waters), as the northern sections of Greenland are bounded by cool polar waters. The same is true for the north sector (Arctic and CAA source waters) for the period of our experiments (2002-2010). As our oceans warm and circulations shift, there may be a potential for an increase of heat content near our northern Greenland sections, amplifying the freshwater anomaly to the sub-Arctic oceans (Karcher *et al.*, 2011; Polyakov *et al.*, 2011; Beszczynska-Mőller *et al.*, 2012; Korhonen *et al.*, 2013).

3.6 Figures and Tables

Table 3.1: Depth Definition: Terminology used to classify the vertical water column of the model.

Terminology	Depth (m)
Surface	0 to 50
Sub-surface	50 to 200
Intermediate	200 to 400
Sub-intermediate	400 to 800
Deep	800 to 1500

ANHA12 ANHA4 REF ANHA4 RUNOFF

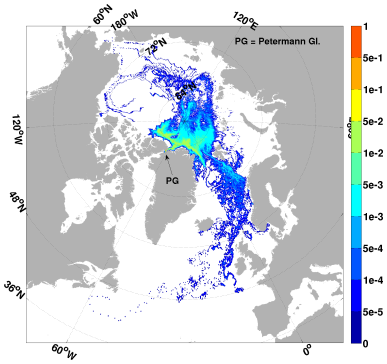

1.a

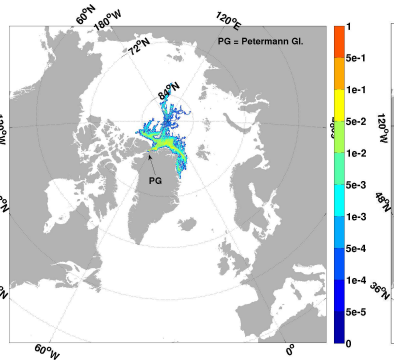

1.b

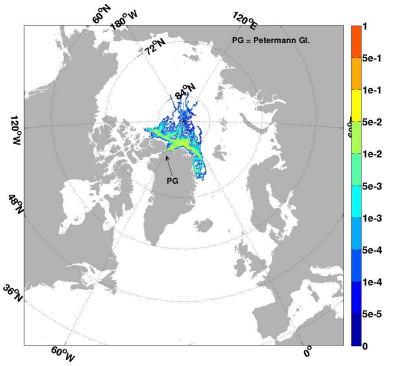

1.c

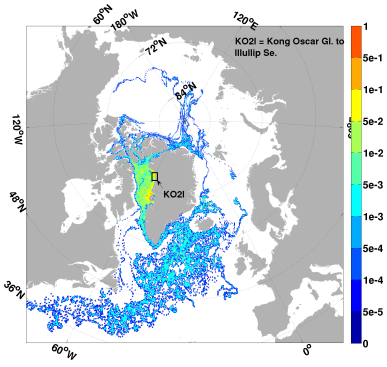

2.a

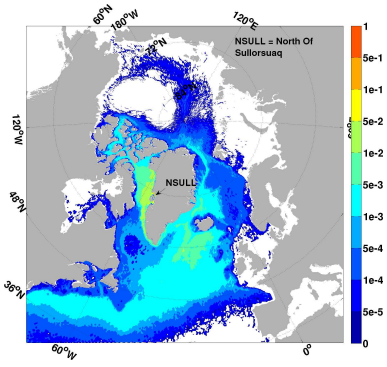

3.a

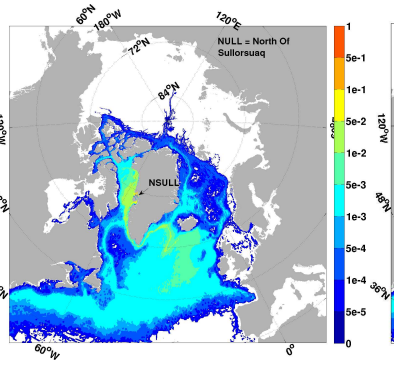

3.b

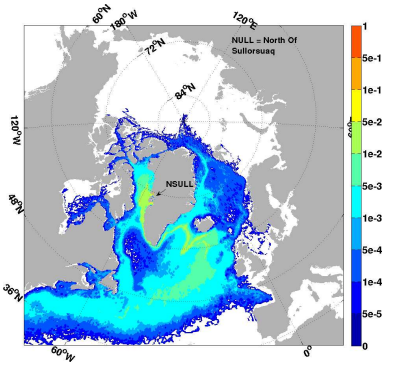

3.c

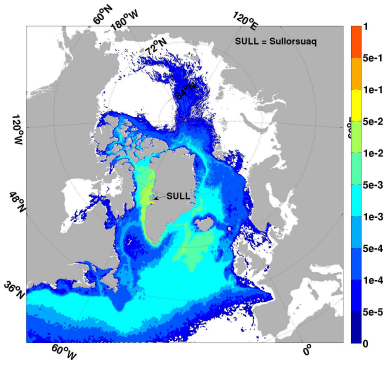

4.a

ANHA12 ANHA4 REF ANHA4 RUNOFF

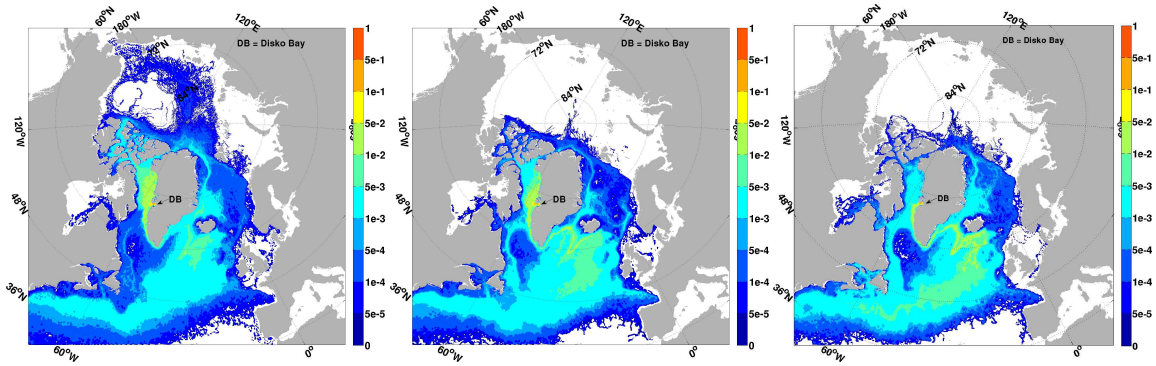

5.a 5.b 5.c

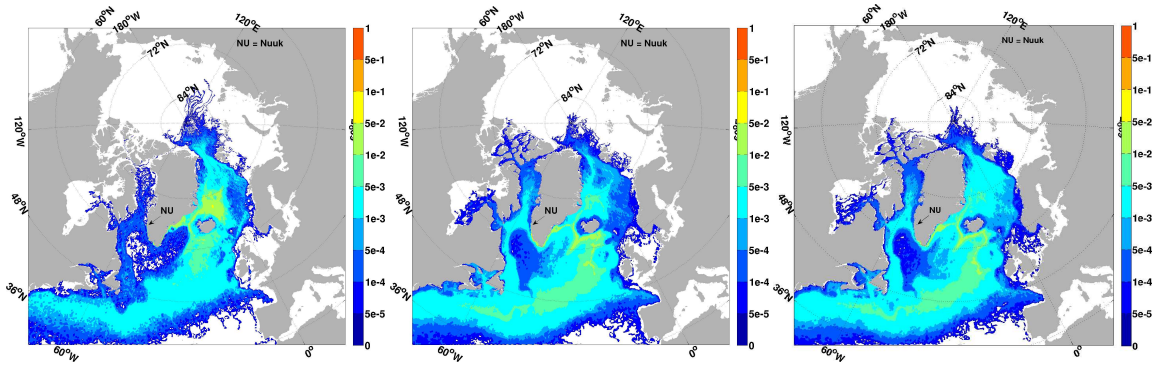

6.a 6.b 6.c

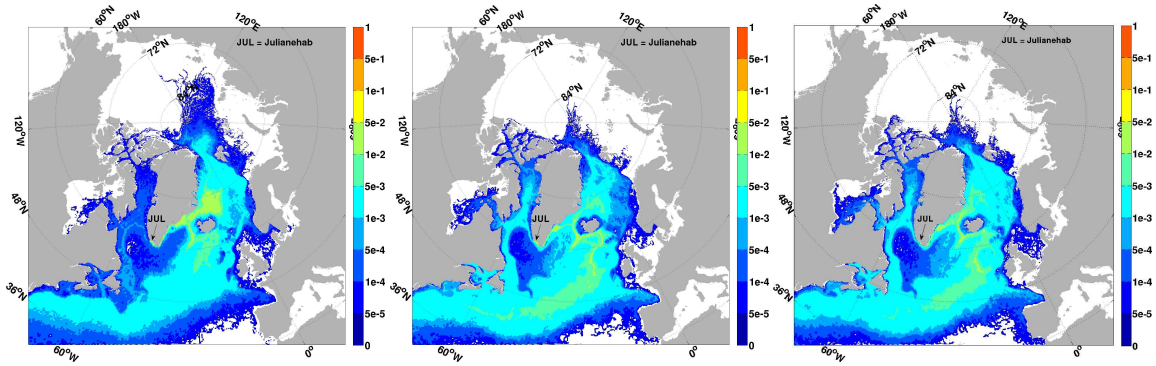

7.a 7.b 7.c

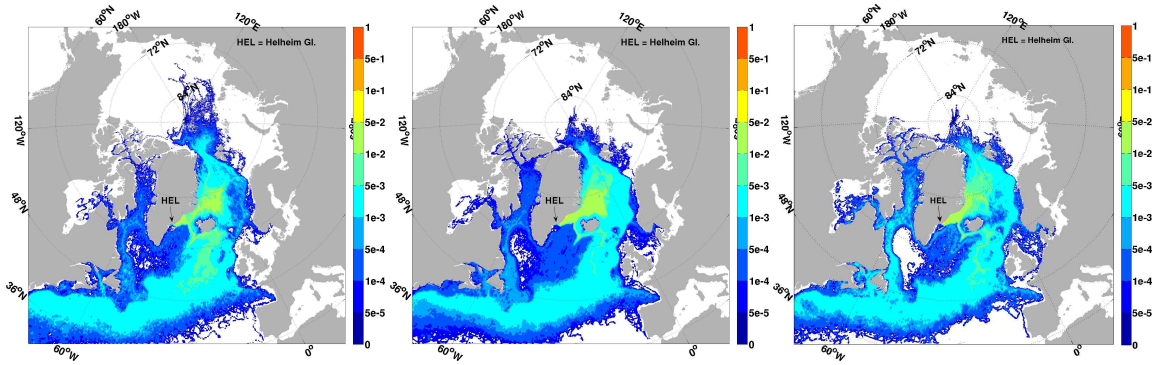

8.a 8.b 8.c

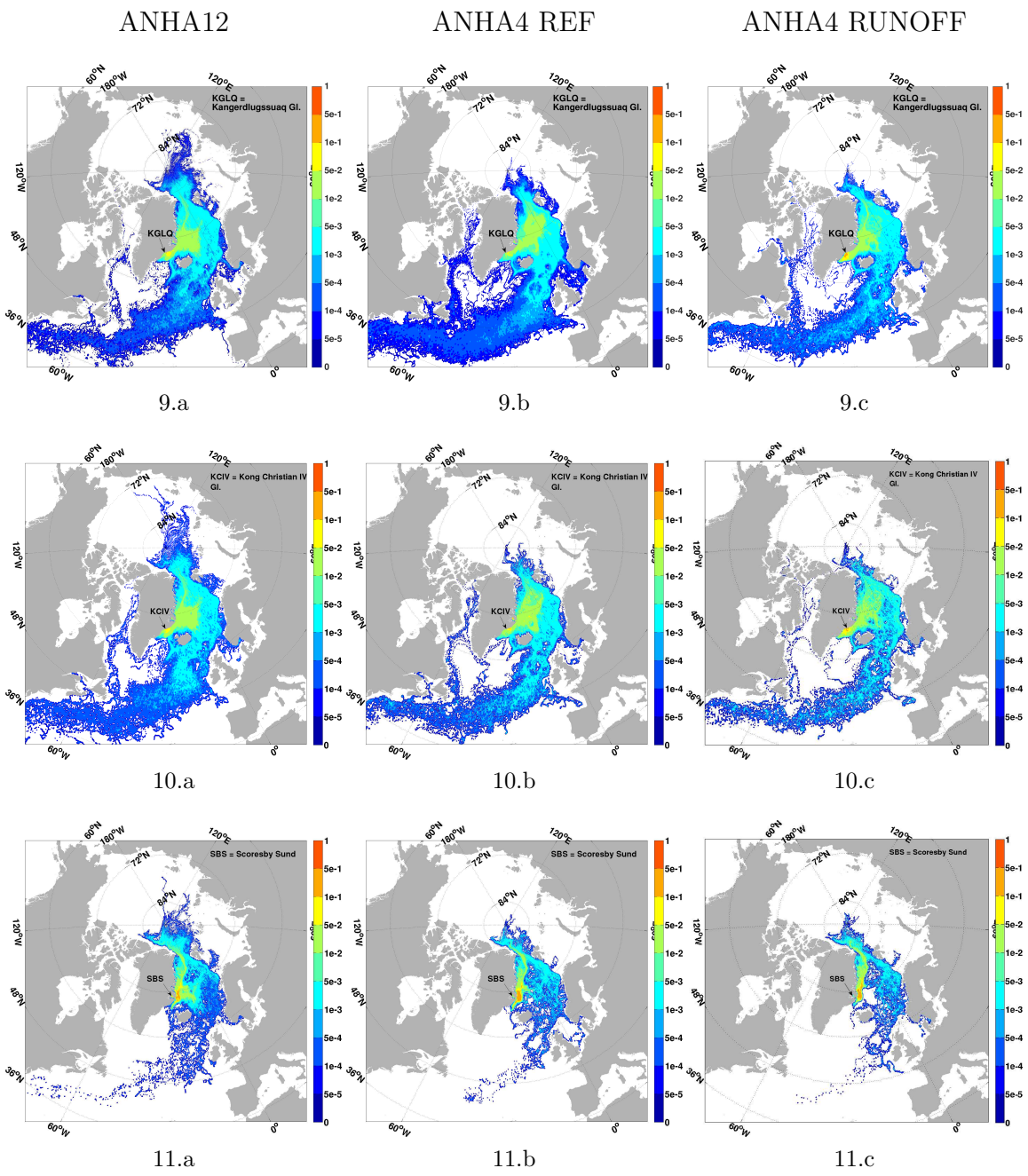

Figure 3.1: Backward probability of 5 year transport of warm water (defined in Table 2.2 with particles initial positions (∼5000) are homogeneously distributed in space and time in each 13 outlet regions (defined in Table 2.3. Every row shares the similar outlet region, noted by the arrow in the figure with the full name on the top right hand side of the figure. Each column separates the outlet region by the 3 experiments (from left to right, ANHA12, ANHA12, ANHA4 REF, ANHA4 RUNOFF). Values here correspond to the percentage out of all floats and grid cells that floats can be found in a given grid cell.

ANHA12 ANHA4 REF ANHA4 RUNOFF

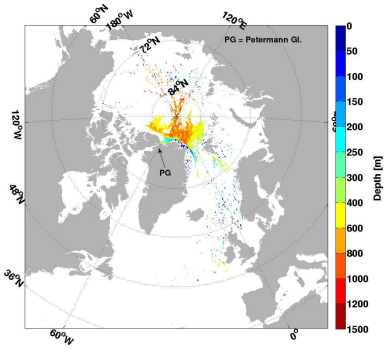

1.a

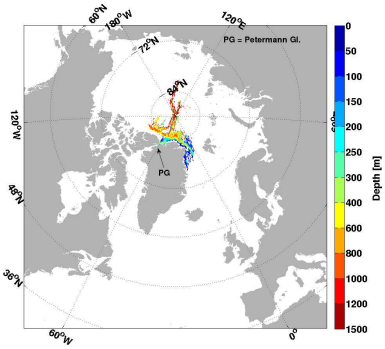

1.b

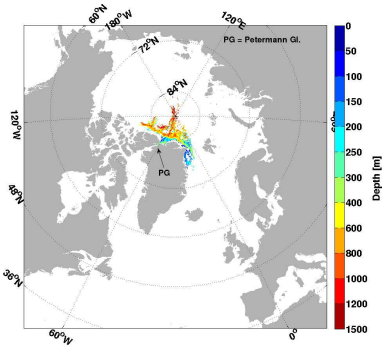

1.c

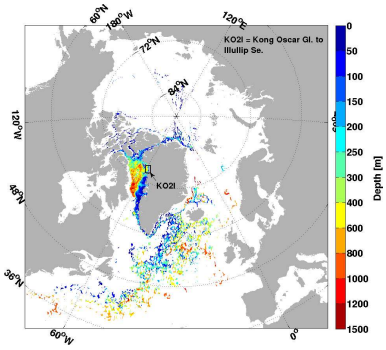

2.a

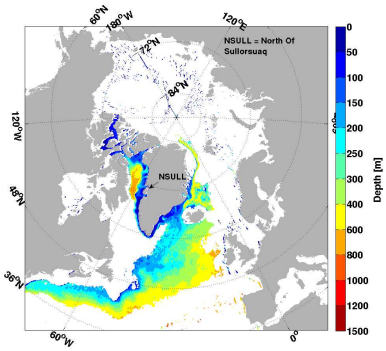

3.a

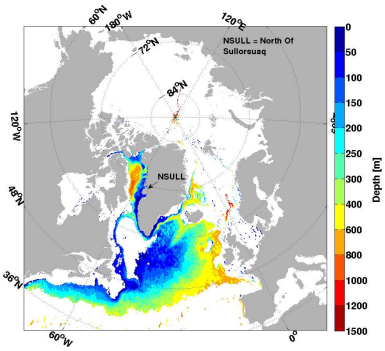

3.b

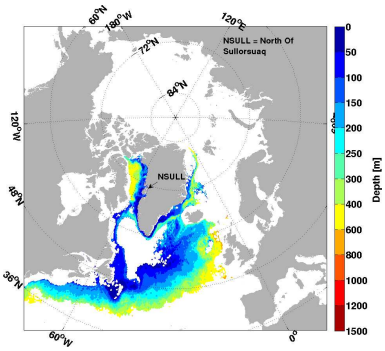

3.c

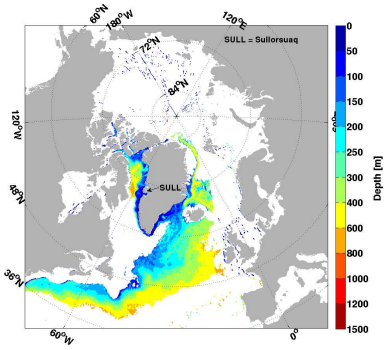

4.a

ANHA12 ANHA4 REF ANHA4 RUNOFF

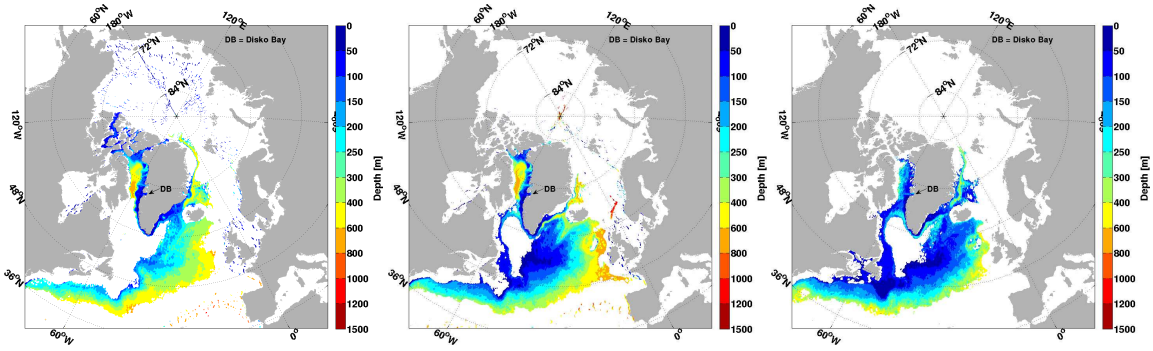

5.a 5.b 5.c

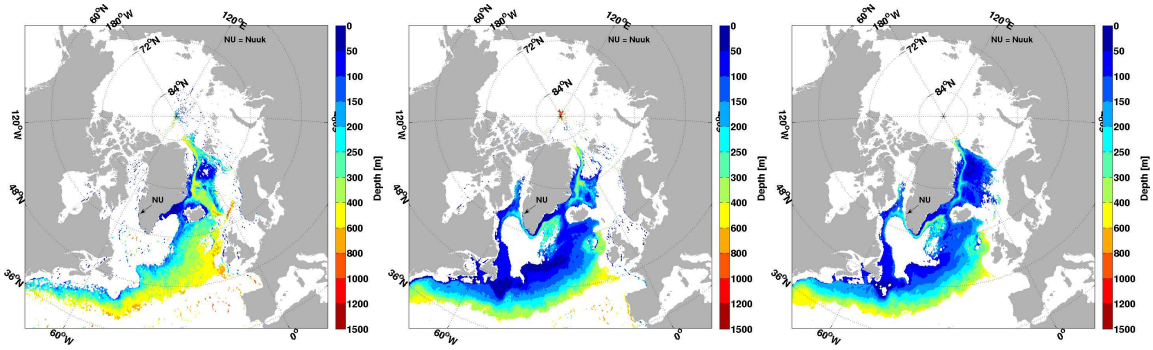

6.a 6.b 6.c

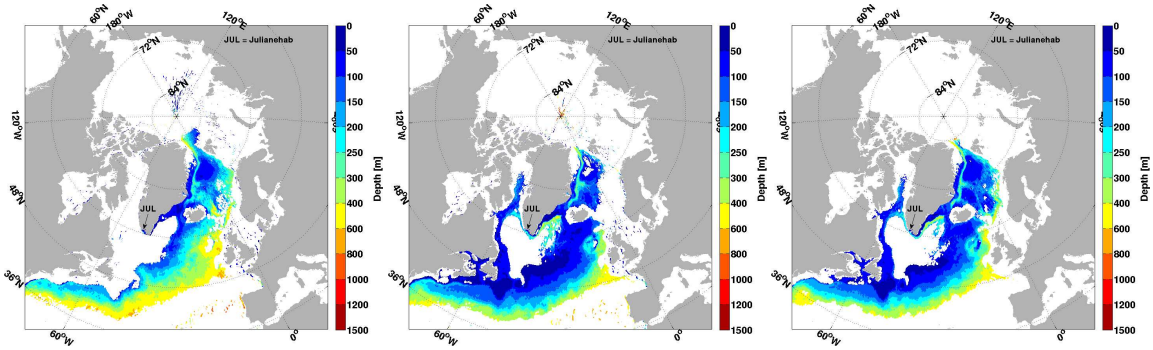

7.a 7.b 7.c

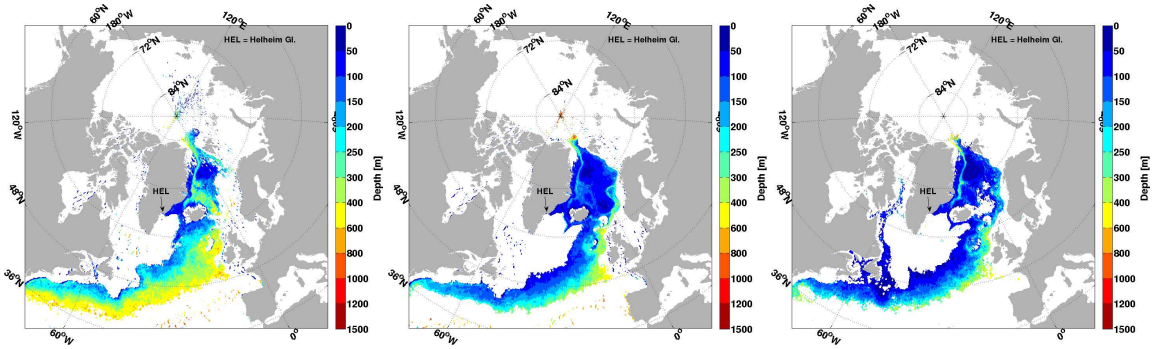

8.a 8.b 8.c

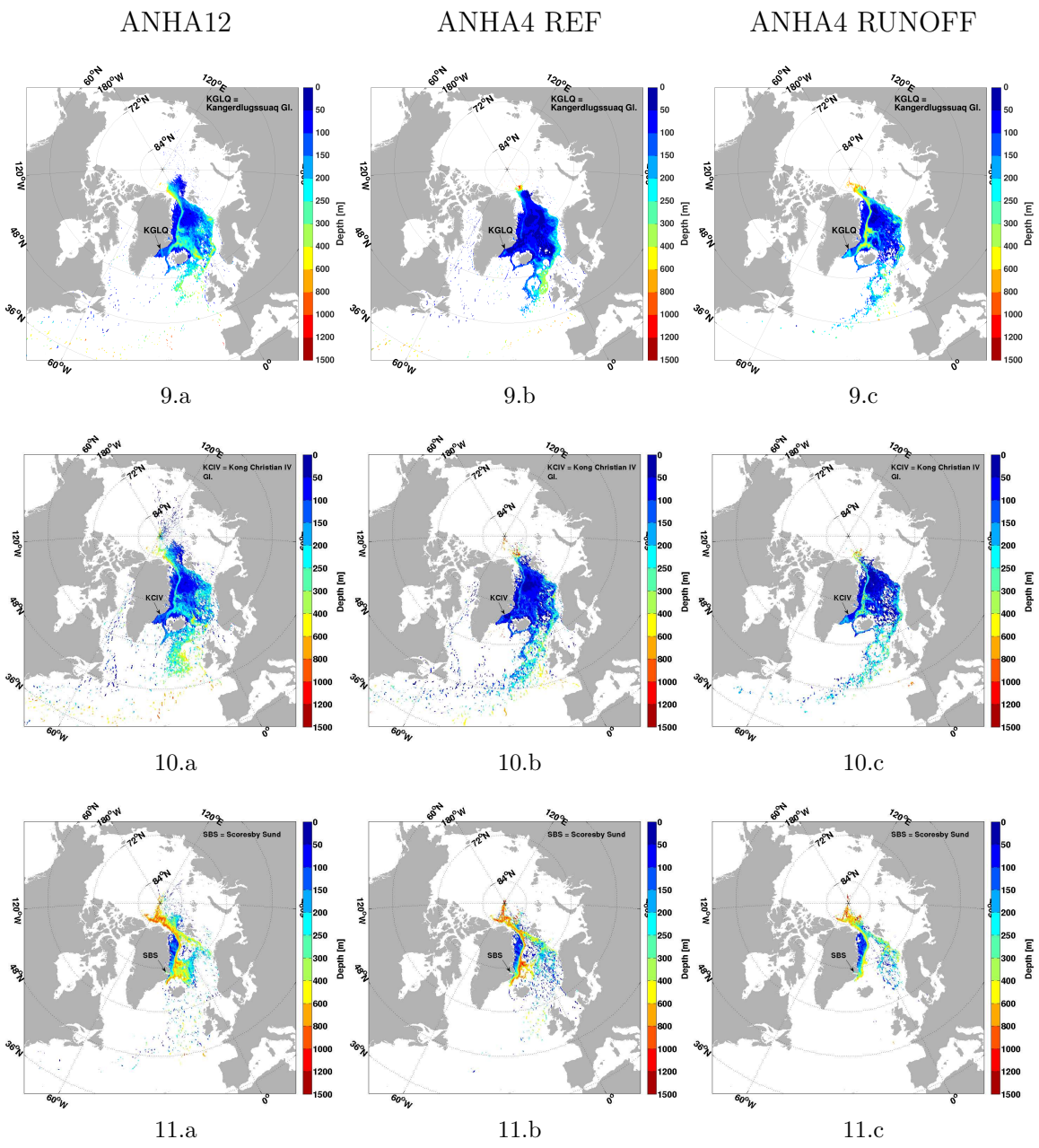

Figure 3.2: Backward depth of medium probability classifcation or higher (Table 2.1) of 5 year transport of warm water (defined in Table 2.2 with particles initial positions (∼5000) are homogeneously distributed in space and time in each 13 outlet regions (defined in Table 2.3. Every row shares the similar outlet region, noted by the arrow in the figure with the full name on the top right hand side of the figure. Each column separates the outlet region by the 3 experiments (from left to right, ANHA12, ANHA12, ANHA4 REF, ANHA4 RUNOFF). Values here correspond to the depth in the water column a particle reached at that grid cell.

ANHA12 ANHA4 REF ANHA4 RUNOFF

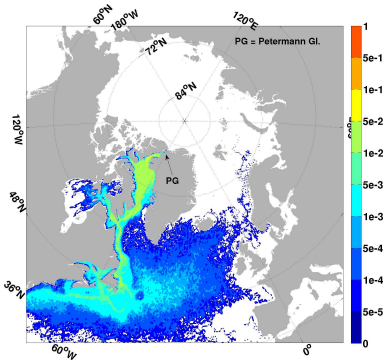

1.a

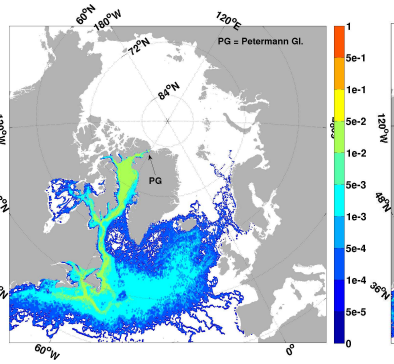

1.b

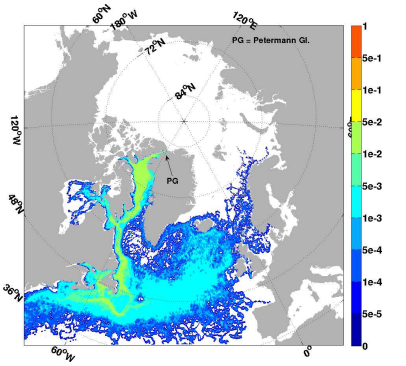

1.c

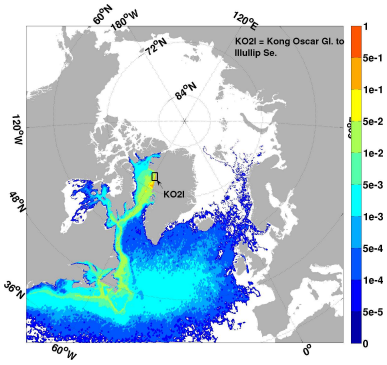

2.a

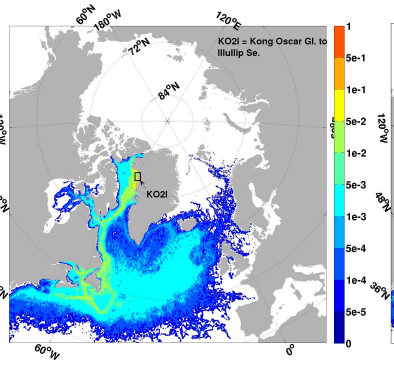

2.b

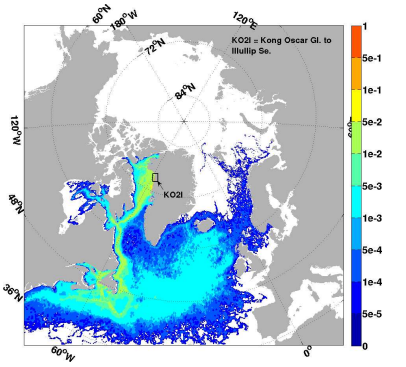

2.c

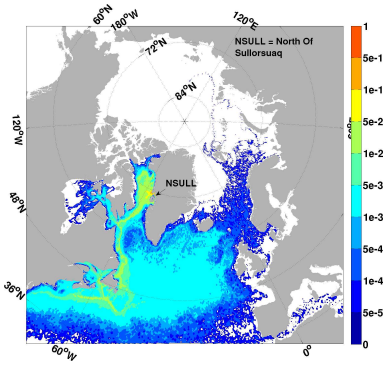

3.a

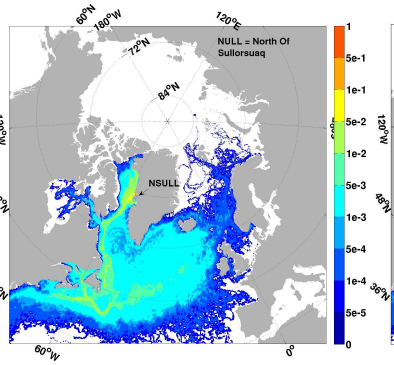

3.b

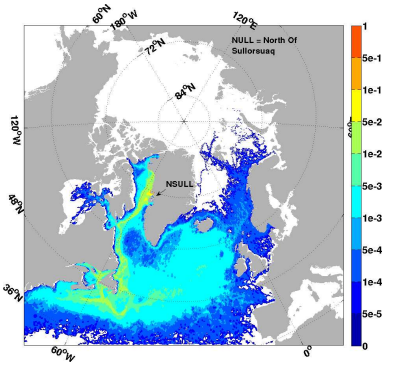

3.c

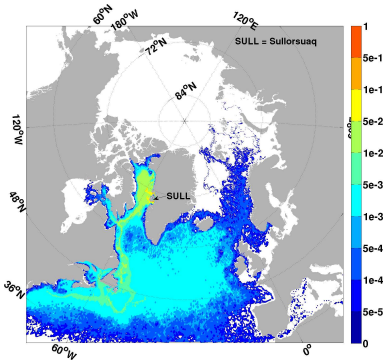

4.a

ANHA12 ANHA4 REF ANHA4 RUNOFF

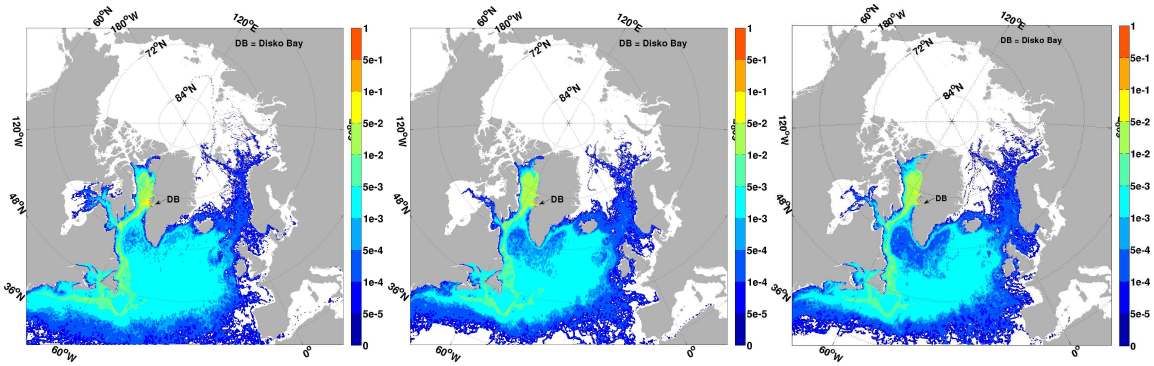

5.a 5.b 5.c

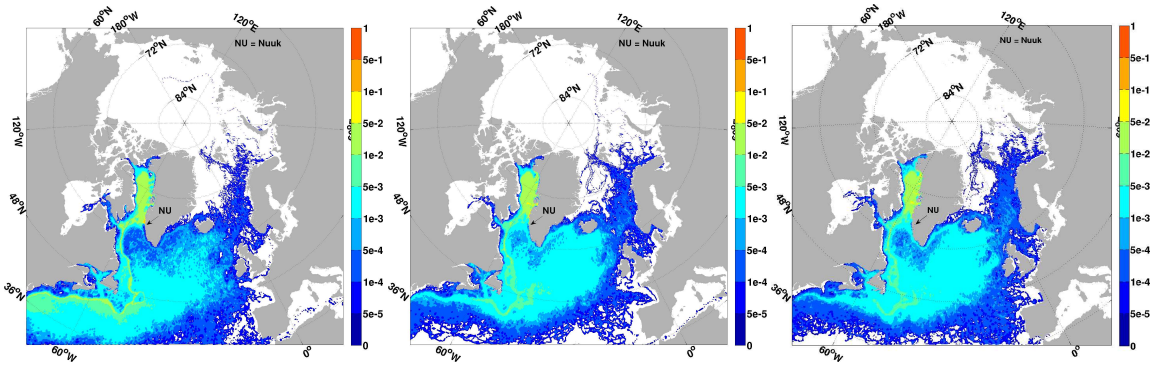

6.a 6.b 6.c

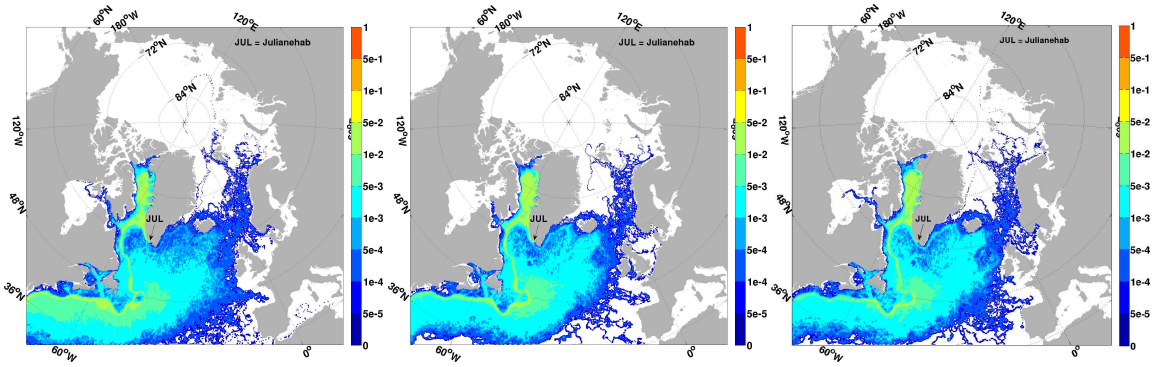

7.a 7.b 7.c

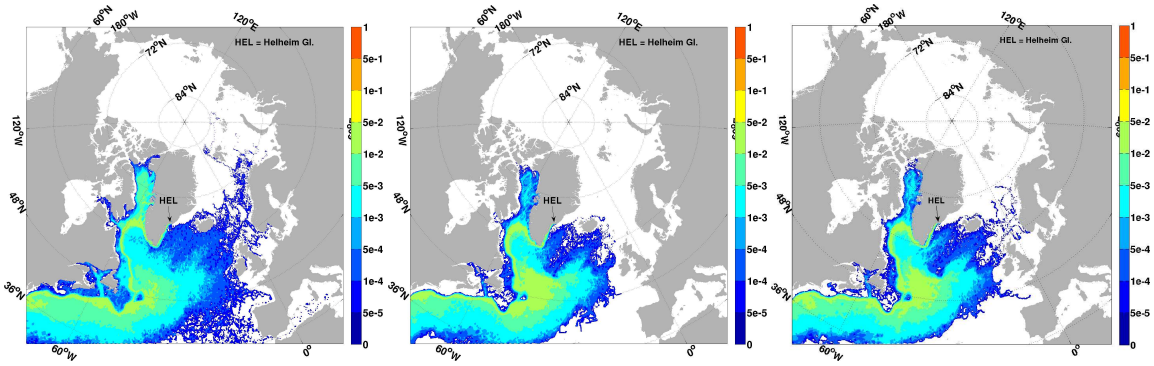

8.a 8.b 8.c

ANHA12 ANHA4 REF ANHA4 RUNOFF

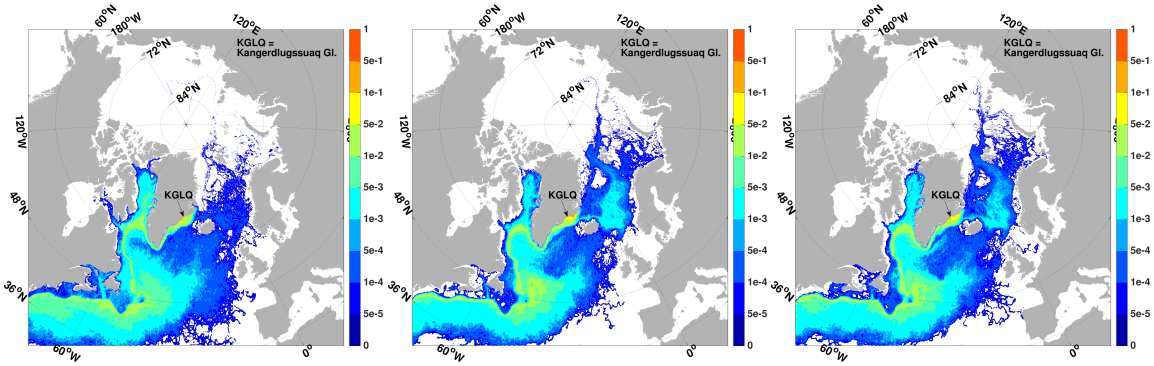

9.a 9.b 9.c

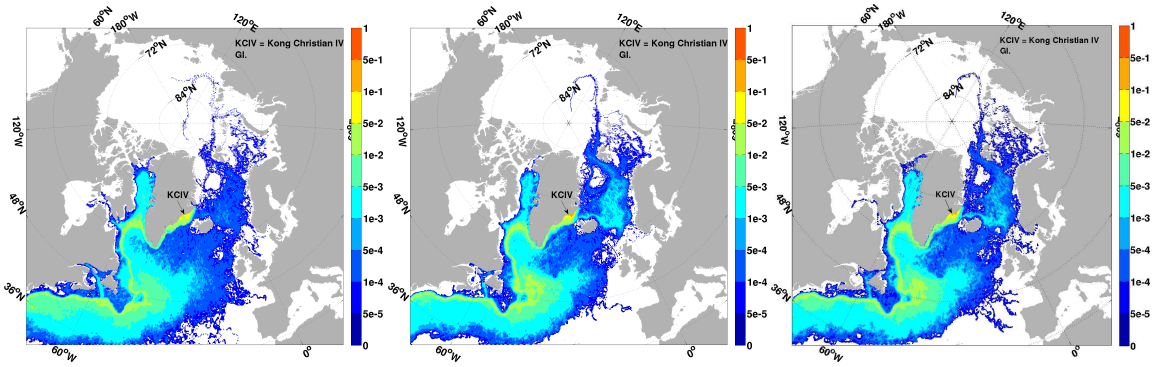

10.a 10.b 10.c

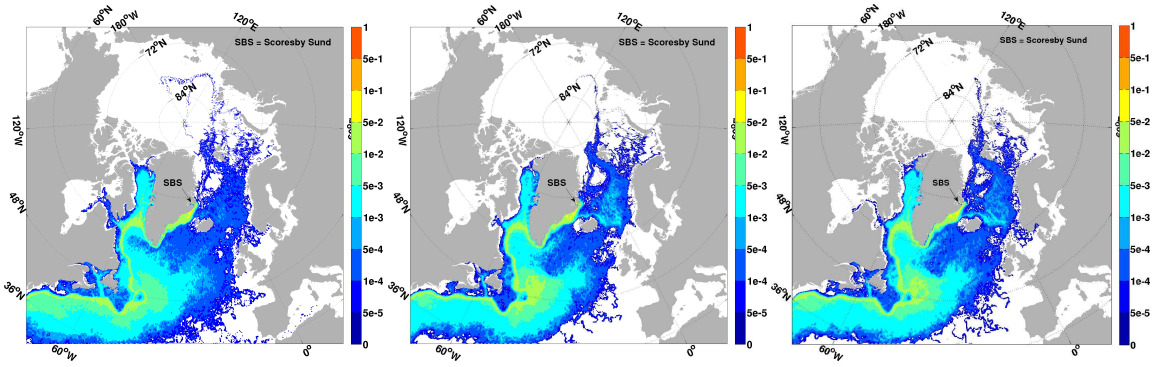

11.a 11.b 11.c

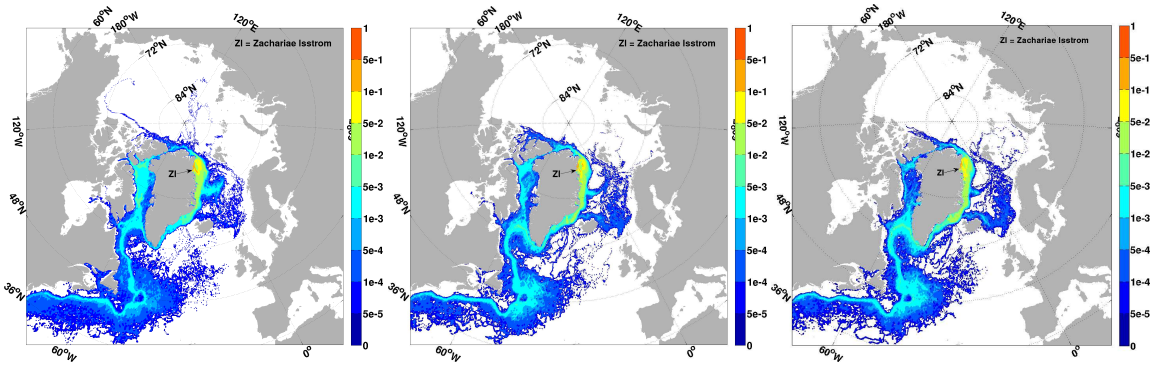

12.a 12.b 12.c

ANHA12 ANHA4 REF ANHA4 RUNOFF

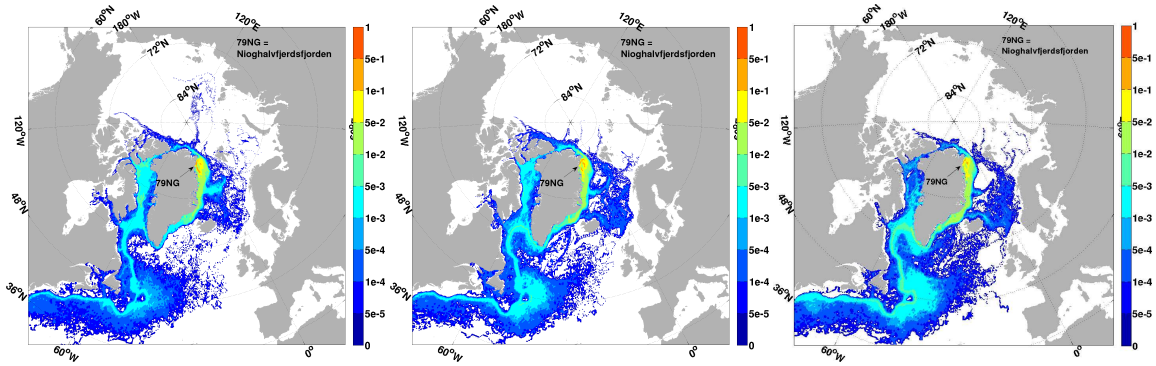

13.a 13.b 13.c

Figure 3.3: Forward probability of 5 year transport of surface water (top 21 vertical model levels with particles initial positions (∼1000) are homogeneously distributed in space and time in the first 21 model grid levels of the water column (77.85 metres). Every row shares the similar outlet region (defined in Table 2.3), noted by the arrow in the figure with the full name on the top right hand side of the figure. Each column separates the outlet region by the 3 experiments (from left to right, ANHA12, ANHA12, ANHA4 REF, ANHA4 RUNOFF). Values here correspond to the percentage out of all floats and grid cells that floats can be found in a given grid cell.

ANHA12 ANHA4 REF ANHA4 RUNOFF

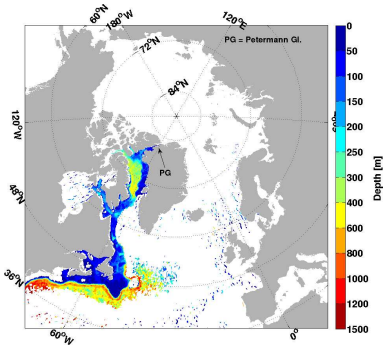

1.a

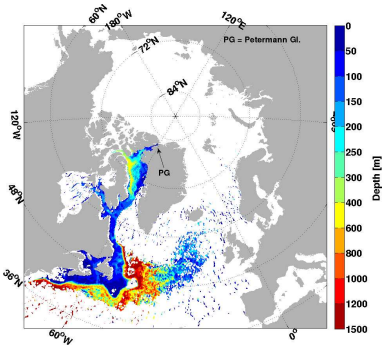

1.b

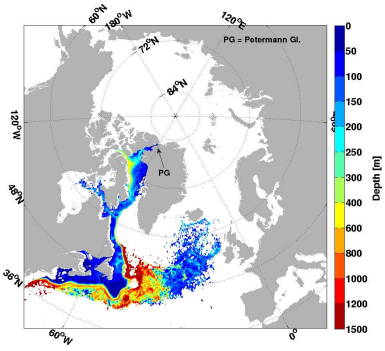

1.c

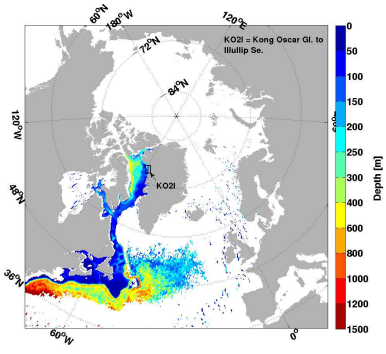

2.a

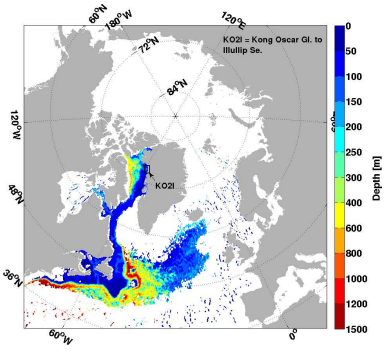

2.b

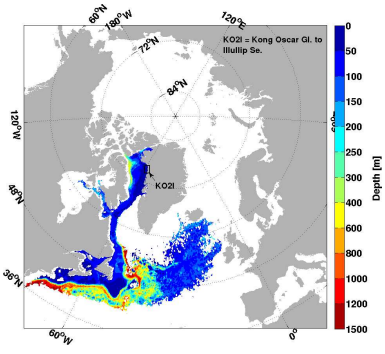

2.c

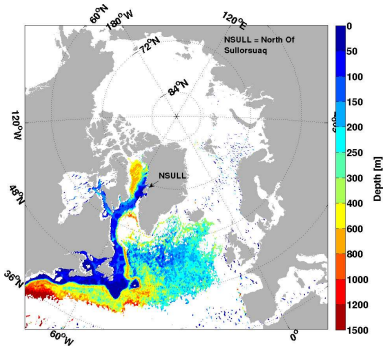

3.a

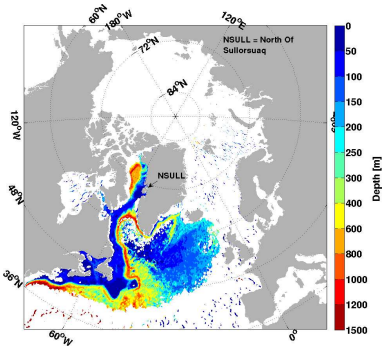

3.b

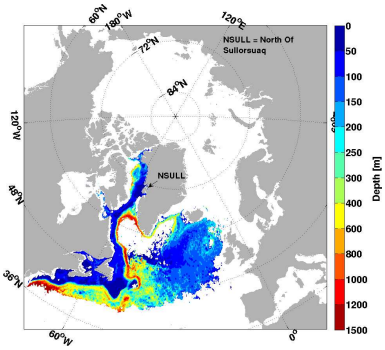

3.c

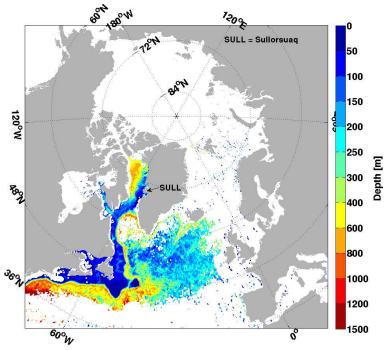

4.a

ANHA12 ANHA4 REF ANHA4 RUNOFF

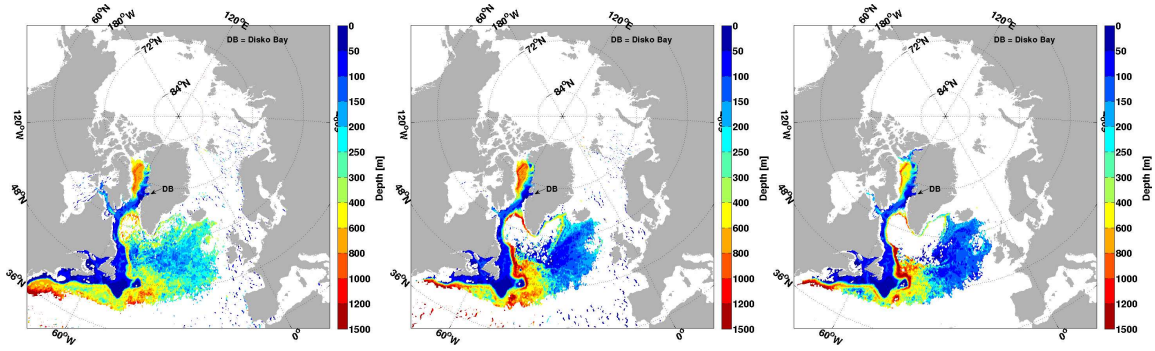

5.a 5.b 5.c

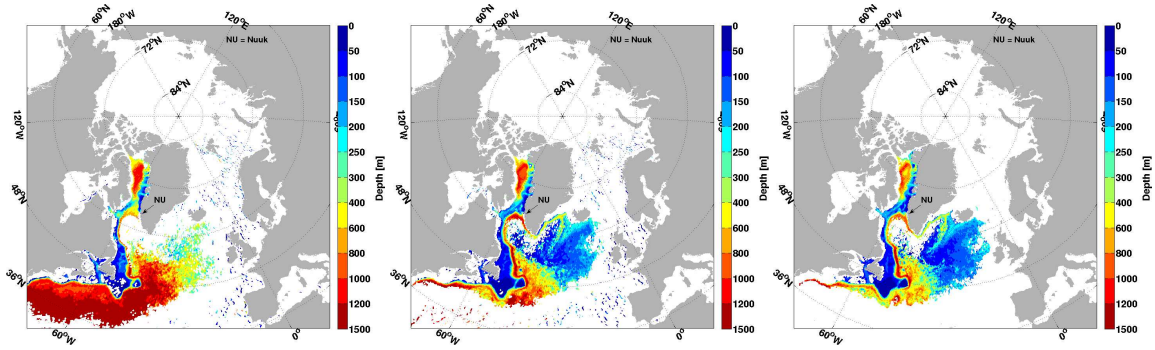

6.a 6.b 6.c

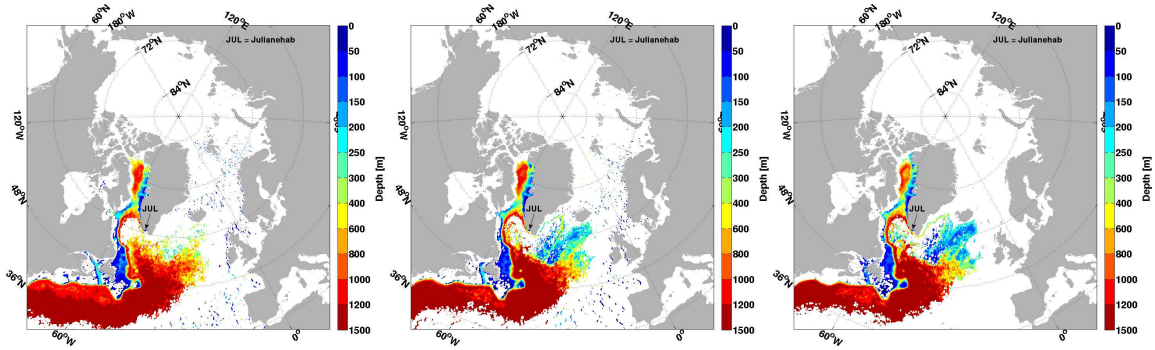

7.a 7.b 7.c

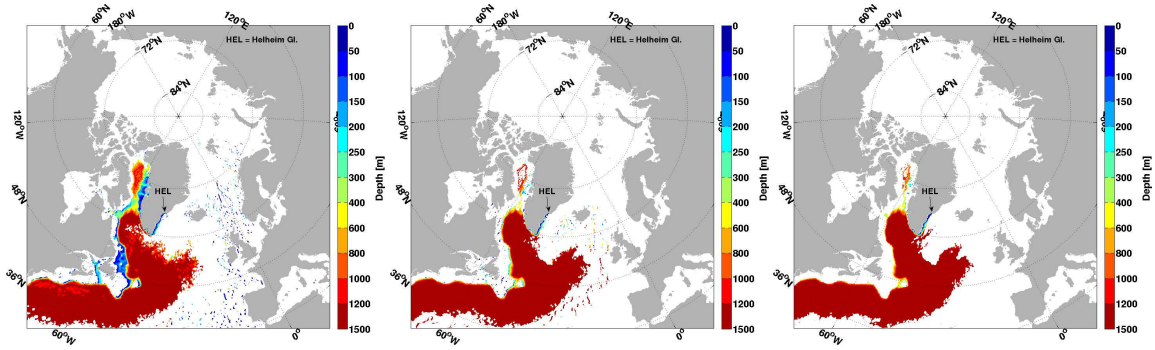

8.a 8.b 8.c

ANHA12 ANHA4 REF ANHA4 RUNOFF

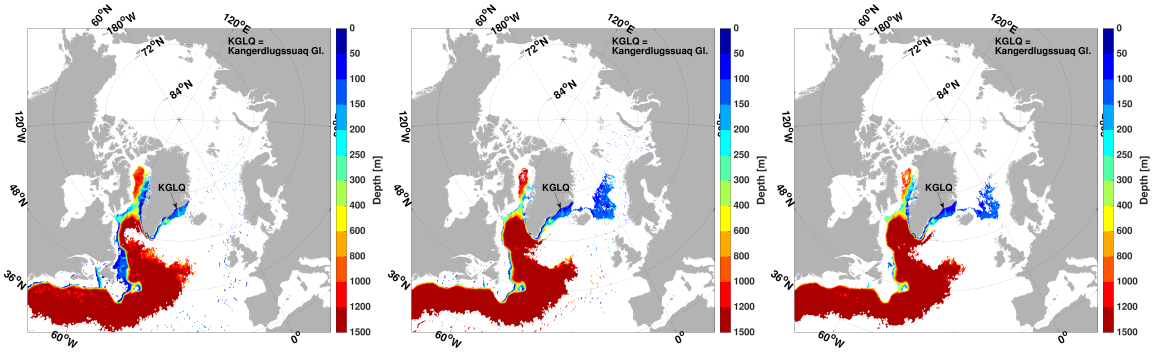

9.a 9.b 9.c

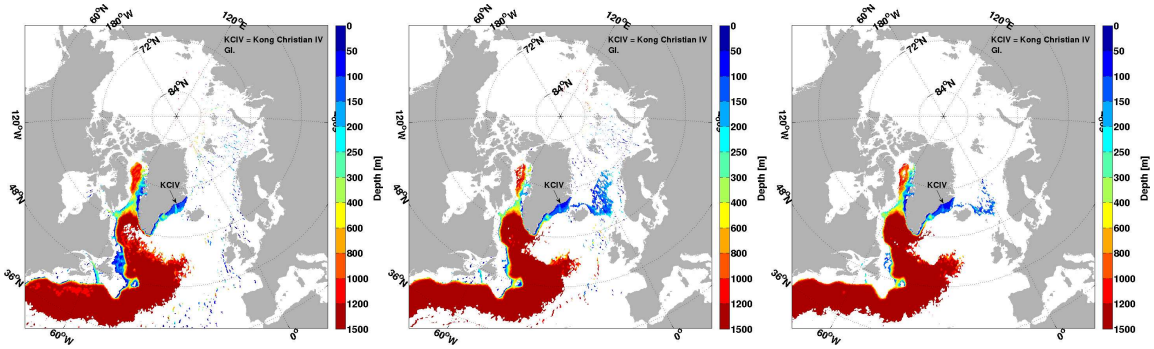

10.a 10.b 10.c

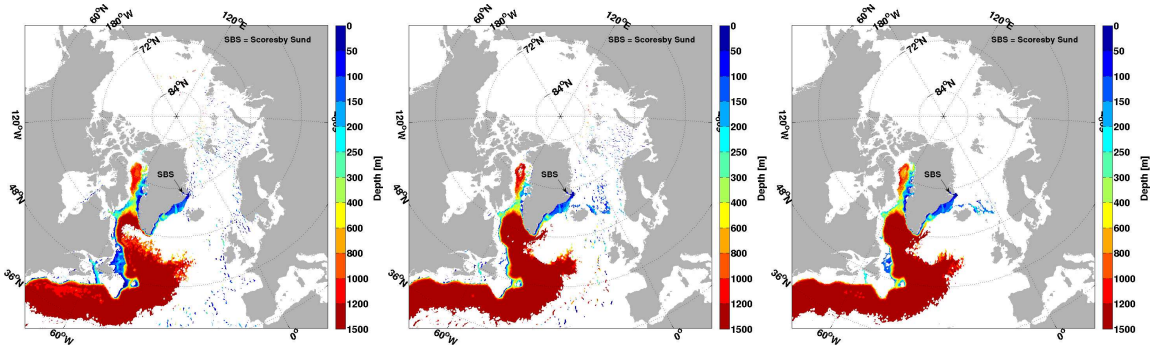

11.a 11.b 11.c

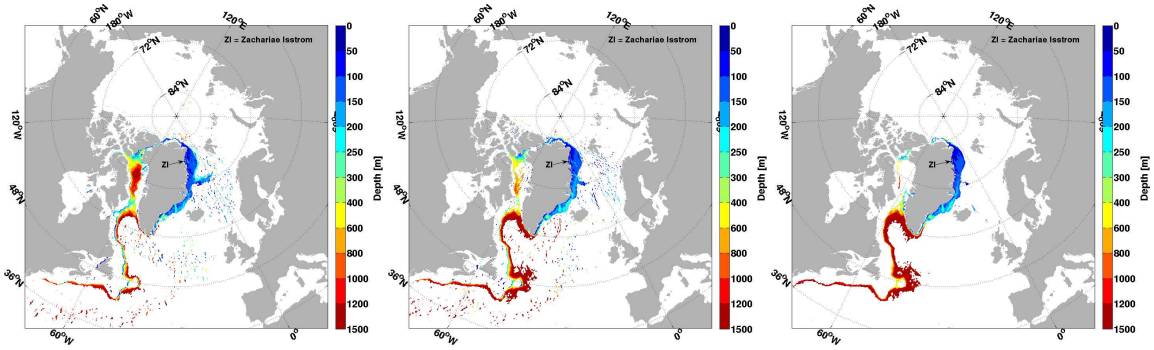

12.a 12.b 12.c

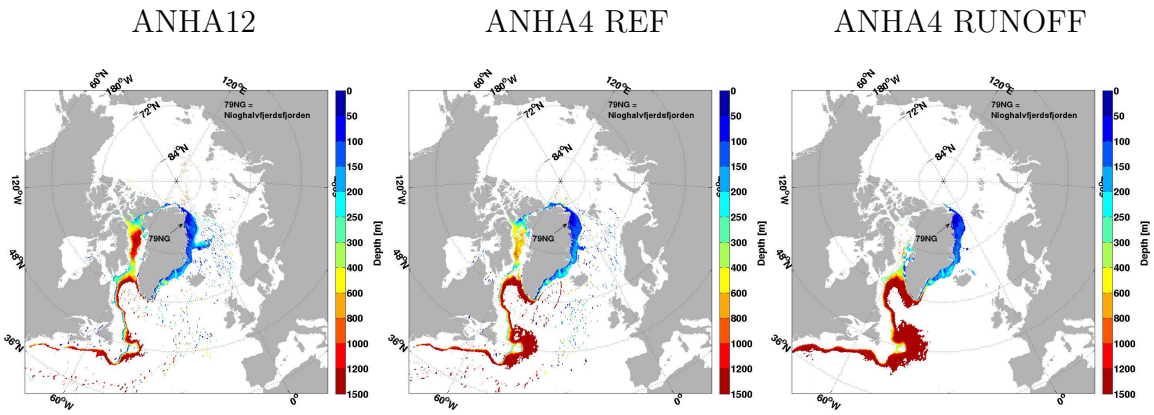

Figure 3.4: Forward depth of medium probability classifcation or higher (Table 2.1) of 5 year transport of surface water (top 21 vertical model levels with particles initial positions (∼1000) are homogeneously distributed in space and time in the first 21 model grid levels of the water column (77.85 metres). Every row shares the similar outlet region (defined in Table 2.3), noted by the arrow in the figure with the full name on the top right hand side of the figure. Each column separates the outlet region by the 3 experiments (from left to right, ANHA12, ANHA12, ANHA4 REF, ANHA4 RUNOFF). Values here correspond to the depth in the water column a particle reached at that grid cell.

Chapter 4

Summary and Conclusions

We were able to locate the origins of warm ocean waters along the Greenland Ice Sheet (GrIS) and how they differ around the island's various coasts due to their location and surrounding ocean circulation. Also we were able to track surface waters, to simulate freshwater, and how they got entrained into surrounding ocean circulation.

Initially during this thesis, we were using older configurations (NEMO-ORCA025 and NEMO-NATL12). ARIANE was compatibly with the former, though the latter ran into more problems. Once our lab group had developed the ANHA configuration, we started to test ARIANE's compatibility. Now 2 years later we have a comparison of the configuration's behaviour with 3 different experiments, all recently created with 3 unique set ups. We were able to compare how a $\frac{1}{4}^o$ and $\frac{1}{12}^o$ resolution experiment compared as well as the question of additional runoff, with ANHA4REF and ANHA4RUNOFF. ANHA12's backward particle trajectories have a tendency to simulate particles coming from further north than any other configuration. This leads to an interesting question: what is the $\frac{1}{4}^o$ resolution not resolving, or is there something unrealistic about the $\frac{1}{12}^o$ experiment's result. ANHA12 captured warmer Arctic Ocean pathways reaching Greenland, whereas ANHA4 con-

figurations did not. Warm water was observed in KO2I for the higher resolution experiment (ANHA12), but not for the coarser resolutions (ANHA4).

Our study was done based on a 5 year analysis, though extending the trajectories longer in time may help answer more questions. Travel time in the Arctic from Fram Strait is around 15 years (Bourgain & Gascard, 2012) and total of 30 years to exit the basin (Karcher *et al.*, 2011; Bourgain & Gascard, 2012). Though once these waters exit, would they still have the heat capacity to melt ice?

Our study has shown that freshwater from north and northwest and southwest Greenland would mix into Baffin Bay by transportation through the West Greenland Current (WGC), as seen in previous studies with coarser resolution (Marsh *et al.*, 2010; Castro de la Guardia *et al.*, 2015). At the southeast regions, including Scoresby Sund (Figure 1.1, the freshwater travelled along the East Greenland Current (EGC) and WGC and has a low likelihood of entering Baffin Bay, instead being directly transported south via Davis Strait into the Labrador Current, which agrees with studies done in Dukhovskoy et al., (in press), showing Greenland freshwater propagating through sub-Arctic seas. Therefore our work alludes to the theory that the high export of freshwater from northwest GrIS (second highest freshwater export on the GrIS (Bamber *et al.*, 2012)) has a higher likelihood of impacting Baffin Bay than all other regions of the GrIS. This freshwater input into Baffin Bay may alter the circulation patterns in Baffin Bay and increase the sea surface height (Marsh *et al.*, 2010; Castro de la Guardia *et al.*, 2015), which may play a role in the future transport of Arctic waters passing through the Canadian Arctic Archipelago (CAA).

The highest freshwater export from the GrIS (southeast section

(Bamber *et al.*, 2012)) will have larger implications for circulation in the North Atlantic Subpolar Gyre (NASPG) and not be as likely to be taken into Baffin Bay, which was not the case in the modelled runoff experiments (with coarser resolution) in Castro de la Guardia (2015). The different results could be from the coarser resolution not being able to resolve mixing from the WGC into the Labrador Sea, as well as different model forcing.

The tracks made from the freshwater paths showed this freshwater from southeast GrIS getting entrained into depths greater than 1000 metres in the interior of the Labrador Sea. Previous studies have analyzed the impact that an increase in freshwater in the interior of the Labrador Sea may reduce the Atlantic Meridonal Overturning Circulation (AMOC) (Belkin *et al.*, 1998; Swingedouw *et al.*, 2006; Myers & Donnelly, 2008; Marsh *et al.*, 2010; Gelderloos *et al.*, 2012; Weijer *et al.*, 2012; Swingedouw *et al.*, 2014). An anomalous event where surface waters increased in buoyancy (in 1968) led to winter convection, shutting down for the next 3 years,the 1970s Great Salinity Anomaly (GSA) (Gelderloos *et al.*, 2012). Our study contributes to the theory and observations as the GrIS continues to melt (as the freshwater anomaly, since 1995, has reached around $\frac{1}{3}$ of the amount of the 1970s GSA (Bamber *et al.*, 2012)), it will have an impact on the AMOC, and has the potential to cause a complete shut down, especially with mild winters which was observed in the 1970s case.(Gelderloos *et al.*, 2012). Freshwater from further northeast (ZI, 79NG) is contained to the East Greenland Coastal Current along the shelf north of Cape Farewell.

Our study agrees with previous observations and models, that warm water comes in close proximity to the northwest coast (Holland *et al.*, 2008; Straneo *et al.*, 2012; Myers & Ribergaard, 2013) and to the south and south east coast of the GrIS (Straneo *et al.*,

2012; Straneo & Heimbach, 2013; Inall *et al.*, 2014; Jackson *et al.*, 2014). Our study takes this one step further and found where the warm waters originated. Warm water came in contact with Petermann Glacier (PG) and Kong Oscar to Illullip Sermia (KO21) were made up of Arctic and CAA waters, where Straneo (2012) found PG to have the coldest warm Atlantic water. Further south at North of Sullorsuaq (NSULL), Sullorsuaq (SULL) and Disko Bay (DB), warmer waters came from Baffin Bay and the Irminger Sea. The Greenland and Nordic Seas become a source of warm waters for the southern coast of Greenland (Nuuk (NU), Julianehab (JUL), Helheim Glacier (HEL)) which were also received warm waters directly from the Irminger Sea via Irminger Current. The Greenland Sea and Nordic Sea become the sole contributor for the transport of warm waters to the east part of Greenland (Kangerdlugssuaq (KGLQ), Kong Christian IV (KCIV), SBS). Straneo (2010) found the warmest Atlantic Water was found by HEL and DB, while we found HEL had two sources of warm water (Greenland/Nordic Sea and Irminger Sea) and DB had Baffin Bay and the Irminger Current. Therefore sections with warm water origins from both the Irminger Current and Greenland/Nordic Seas may have the highest heat content.

The next in Straneo's (2010) study to have the warmest Atlantic Water was KGLQ (which we found is fed from the Greenland and Nordic Seas) and then Nioghalvfjerdsfjorden (79NG), where our experiments could not pick up warm waters along the north east portion of Greenland (Zachariae Isstrom (ZI) and 79NG). Comparing with observations (Rhein, personal communication, September 6th, 2015) personal communications), observations have shown warm waters reaching 79NG. Therefore, we need to further examine the complex circulation along the east Greenland Shelf to compare the

varying results.

Oceanic heat may not be playing a large role in the northeast sector of the GrIS (where our experiments could not resolve warm waters), as the northern sections of Greenland are bounded by cool polar waters. The same is true for the north sector (Arctic and CAA source waters) for the period of our experiments (2002-2010). As our oceans warm and circulations shift, there may be a potential for an increase of heat content near our northern Greenland sections, amplifying the freshwater anomaly to the sub-Arctic oceans (Karcher *et al.*, 2011; Polyakov *et al.*, 2011; Beszczynska-Mőller *et al.*, 2012; Korhonen *et al.*, 2013).

Using ARIANE offline from our NEMO configuration raises the question about accuracy of diffusion and mixing processes, as the ocean model does this while ARIANE does not. A previous study used ARIANE to simulate ocean pathways, the errors and overestimation's were concluded to be an error with the Eulerain fields, not the Lagrangian calculation (Lique *et al.*, 2010). We know some limitations with our model, such as a salinity drift and issues with the mixed layer depth within the Labrador Sea being deeper than observations during winter convection. As well, further examination needs to be done on the accuracy of simulating ocean circulation along the east Greenland shelf, as our experiments did not find warm waters by the 79NG glacier, which contrasts to observations (Rhein, 2015, personal communication). That being said, ARIANE greatly reduced the computational cost, since we previously ran the model and then applied the particle tracking tool. I was able to apply ARIANE to older configurations at first, and then once new configurations were created and tested, we experimented with running ARIANE, and found it compatible between all experiments. The freedom to add more tests and configurations was appreciated

and the time spent running the program fit well for a Masters thesis. I would like to have compared a larger time series and look at the evolution of the some of the circulation patterns.

In the future, for researchers using ARIANE, I would advise to use an experiment with good representation of runoff, as buoyancy and mixing had a major impact on the particle trajectories. With a higher resolution, one could take a look at tracking warm waters that enter the straits of the CAA, and see if ocean heat may play a role in the decreasing ice caps on the islands. Another idea that comes to mind that I would have liked to included would be to increase the coastal resolution to simulate accurate fjord mixing. Comparing this study with a passive tracer run online would be fascinating to see the differences between the offline and online approaches.

Bibliography

Aagaard, K. & Carmack, E. C. 1989 The role of sea ice and other fresh water in the arctic circulation. *Journal of Geophysical Research: Oceans* **94** (C10), 14485–14498.

Aksenov, Y., Bacon, S., Coward, A. C. & Holliday, N. P. 2010 Polar outflow from the arctic ocean: A high resolution model study. *Journal of Marine Systems* **83** (12), 14 – 37.

Bacon, S., Marshall, A., Holliday, N. P., Aksenov, Y. & Dye, S. R. 2014 Seasonal variability of the east greenland coastal current. *Journal of Geophysical Research: Oceans* **119** (6), 3967–3987.

Bamber, J., Van Den Broeke, M., Ettema, J., Lenaerts, J. & Rignot, E. 2012 Recent large increases in freshwater fluxes from greenland into the north atlantic. *Geophysical Research Letters* **39** (19).

Belkin, I., Levitus, S., Antonov, J. & Malmberg, S.-A. 1998 'great salinity anomalies' in the north atlantic. *Progress in Oceanography* **41** (1), 1–68, cited By 0.

Beszczynska-Mőller, A., Fahrbach, E., Schauer, U. & Hansen, E. 2012 Variability in atlantic water temperature and transport at the entrance to the arctic ocean, 19972010. *ICES Journal of Marine Science: Journal du Conseil* .

Blanke, B. & Grima, N. 2008 Tutorial: first steps with ariane, sequential version.

Blanke, B. & Raynaud, S. 1997 Kinematics of the pacific equatorial undercurrent: An eulerian and lagrangian approach from gcm results. *Journal of Physical Oceanography* **27** (6), 1038–1053.

Bourgain, P. & Gascard, J. C. 2012 The atlantic and summer pacific waters variability in the arctic ocean from 1997 to 2008. *Geophysical Research Letters* **39** (5), n/a–n/a, l05603.

Box, J. E., Bromwich, D. H., Veenhuis, B. A., Bai, L. ., Stroeve, J. C., Rogers, J. C., Steffen, K., Haran, T. & Wang, S. . 2006 Greenland ice sheet surface mass balance variability (1988-2004) from calibrated polar mm5 output. *Journal of Climate* **19** (12), 2783–2800.

Christoffersen, P., Mugford, R. I., Heywood, K. J., Joughin, I., Dowdeswell, J. A., Syvitski, J. P. M., Luckman, A. & Benham, T. J. 2011 Warming of waters in an east greenland fjord prior to glacier retreat: Mechanisms and connection to large-scale atmospheric conditions. *Cryosphere* **5** (3), 701–714.

Dai, A., Qian, T., Trenberth, K. E. & Milliman, J. D. 2009 Changes in continental freshwater discharge from 1948 to 2004. *Journal of Climate* **22** (10), 2773–2792.

Dickson, R., Rudels, B., Dye, S., Karcher, M., Meincke, J. & Yashayaev, I. 2007 Current estimates of freshwater flux through arctic and subarctic seas. *Progress in Oceanography* **73** (3-4), 210–230.

DRAKKAR, Barnier, B., L., B., J., L. S., J.-M., M., T., P., S., T., M., T. A., G., M., A., B., C., B., J., D., S., G., R., B. B., J., C., G., G., S., A., A., C., de Cuevas B., A., N., K., H., G., S., S., D., W., H., C., S. & P., M. 2007 Eddy-permitting ocean circulation hindcasts of past decades. *CLIVAR Exchanges* **12** (3), 8–10.

Dukhovskoy, D., Myers, P., Platov, G., Timmermans, M., Proshutinksy, A., Curry, B., Bamber, J., Chassignet, E., Hu, X., Lee, C. & Somavilla, R. submitted Greenland freshwater in the sub-arctic seas from model experiments with passive tracers.

Enderlin, E. M., Howat, I. M., Jeong, S., Noh, M. ., Van Angelen, J. H. & Van Den Broeke, M. R. 2014 An improved mass budget for the greenland ice sheet. *Geophysical Research Letters* **41** (3), 866–872.

Ferry, N., Greiner, E., Garric, G., Penduff, T., Treiguier, A.-M. & Reverdin, G. 2008 Glorys-1 reference manual for stream 1 (2002-2007). GLORYS project report.

Ferry, N., Parent, L., Garric, G., Drevillon, M., Desportes, C., Bricaud, C. & Hernadez, F. 2012 Scientific validation report (scvr) for reprocessed analysis and reanalysis. MyOcean project report.

Fichefet, T. & Morales Maqueda, M. 1997 Sensitivity of a global sea ice model to the treatment of ice thermodynamics and dynamics. *Journal of Geophysical Research* **102** (C6), 12609–12646, cited By 334.

Fichefet, T., Poncin, C., Goosse, H., Huybrechts, P., Janssens, I. & Le Treut, H. 2003 Implications of changes in

freshwater flux from the greenland ice sheet for the climate of the 21st century. *Geophysical Research Letters* **30** (17), CLM 8–1 – 8–4.

Fratantoni, P. S. & Pickart, R. S. 2007 The western north atlantic shelfbreak current system in summer. *Journal of Physical Oceanography* **37** (10), 2509–2533.

Gelderloos, R., Straneo, F. & Katsman, C. 2012 Mechanisms behind the temporary shutdown of deep convection in the labrador sea: Lessons from the great salinity anomaly years 1968-71. *Journal of Climate* **25** (19), 6743–6755, cited By 0.

Gladish, C., Holland, D. & Lee, C. 2015 Oceanic boundary conditions for jakobshavn glacier. part ii: Provenance and sources of variability of disko bay and ilulissat icefjord waters, 1990-2011. *Journal of Physical Oceanography* **45** (1), 33–63, cited By 0.

Castro de la Guardia, L., Hu, X. & Myers, P. G. 2015 Potential positive feedback between greenland ice sheet melt and baffin bay heat content on the west greenland shelf. *Geophysical Research Letters* **42** (12), 4922–4930, 2015GL064626.

Hanna, E., Navarro, F. J., Pattyn, F., Domingues, C. M., Fettweis, X., Ivins, E. R., Nicholls, R. J., Ritz, C., Smith, B., Tulaczyk, S., Whitehouse, P. L. & Jay Zwally, H. 2013 Ice-sheet mass balance and climate change. *Nature* **498** (7452), 51–59.

Holland, D. M., Thomas, R. H., De Young, B., Ribergaard, M. H. & Lyberth, B. 2008 Acceleration of jakobshavn isbr triggered by warm subsurface ocean waters. *Nature Geoscience* **1** (10), 659–664.

Hu, X. 2015, personal communication .

Inall, M. E., Murray, T., Cottier, F. R., Scharrer, K., Boyd, T. J., Heywood, K. J. & Bevan, S. L. 2014 Oceanic heat delivery via kangerdlugssuaq fjord to the south-east greenland ice sheet. *Journal of Geophysical Research: Oceans* **119** (2), 631–645.

Jackson, R. H., Straneo, F. & Sutherland, D. A. 2014 Externally forced fluctuations in ocean temperature at greenland glaciers in non-summer months. *Nature Geoscience* **7** (7), 503–508.

Jenkins, A. 2011 Convection-driven melting near the grounding lines of ice shelves and tidewater glaciers. *Journal of Physical Oceanography* **41** (12), 2279–2294.

Karcher, M., Beszczynska-Mller, A., Kauker, F., Gerdes, R., Heyen, S., Rudels, B. & Schauer, U. 2011 Arctic ocean warming and its consequences for the denmark strait overflow. *Journal of Geophysical Research: Oceans* **116** (C2), n/a–n/a.

Korhonen, M., Rudels, B., Marnela, M., Wisotzki, A. & Zhao, J. 2013 Time and space variability of freshwater content, heat content and seasonal ice melt in the arctic ocean from 1991 to 2011. *Ocean Science* **9** (6), 1015–1055.

Large, W. G. & Yeager, S. G. 2008 The global climatology of an interannually varying air - sea flux data set. *Climate Dynamics* **33** (2-3), 341–364.

Lique, C., Treguier, A. M., Blanke, B. & Grima, N. 2010 On the origins of water masses exported along both sides of green-

land: A lagrangian model analysis. *Journal of Geophysical Research: Oceans* **115** (C5), n/a–n/a.

Madec, G. 2008 Nemo ocean engine.

Marsh, R., Desbruyres, D., Bamber, J., De Cuevas, B., Coward, A. & Aksenov, Y. 2010 Short-term impacts of enhanced greenland freshwater fluxes in an eddy-permitting ocean model. *Ocean Science* **6** (3), 749–760, cited By 0.

Marshall, J., Dobson, F., Moore, K., Rhines, P., Visbeck, M., D'Asaro, E., Bumke, K., Chang, S., Davis, R., Fischer, K., Garwood, R., Guest, P., Harcourt, R., Herbaut, C., Holt, T., Lazier, J., Legg, S., McWilliams, J., Pickart, R., Prater, M., Renfrew, I., Schott, F., Send, U. & Smethie, W. 1998 The labrador sea deep convection experiment. *Bulletin of the American Meteorological Society* **79** (10), 2033–2058, cited By 0.

Melling, H., Agnew, T. A., Falkner, K. K., Greenberg, D. A., Lee, C. M., Mnchow, A., Petrie, B., Prinsenberg, S. J., Samelson, R. M. & Woodgate, R. A. 2008 Freshwater fluxes via pacific and arctic outflows across the canadian polar shelf. *Arctic-Subarctic Ocean Fluxes: Defining the Role of the Northern Seas in Climate* pp. 193–247.

Myers, P. & Donnelly, C. 2008 Water mass transformation and formation in the labrador sea. *Journal of Climate* **21** (7), 1622–1638, cited By 12.

Myers, P. G., Donnelly, C. & Ribergaard, M. H. 2009 Structure and variability of the west greenland current in summer derived from 6 repeat standard sections. *Progress in Oceanography* **80** (1-2), 93–112.

Myers, P. G. & Ribergaard, M. H. 2013 Warming of the polar water layer in disko bay and potential impact on jakobshavn isbrae. *Journal of Physical Oceanography* **43** (12), 2629–2640.

Polyakov, I., Alexeev, V., Ashik, I., Bacon, S., Beszczynska-Mller, A., Carmack, E., Dmitrenko, I., Fortier, L., Gascard, J.-C., Hansen, E., Hlemann, J., Ivanov, V., Kikuchi, T., Kirillov, S., Lenn, Y.-D., McLaughlin, F., Piechura, J., Repina, I., Timokhov, L., Walczowski, W. & Woodgate, R. 2011 Fate of early 2000s arctic warm water pulse. *Bulletin of the American Meteorological Society* **92** (5), 561–566, cited By 34.

Rhein, M. 2015, personal communication .

Rignot, E. & Kanagaratnam, P. 2006 Changes in the velocity structure of the greenland ice sheet. *Science* **311** (5763), 986–990.

Rignot, E. & Mouginot, J. 2012 Ice flow in greenland for the international polar year 2008-2009. *Geophysical Research Letters* **39** (11).

Rudels, B. 2015 Arctic ocean circulation, processes and water masses: A description of observations and ideas with focus on the period prior to the international polar year 20072009. *Progress in Oceanography* **132** (0), 22 – 67, oceanography of the Arctic and North Atlantic Basins.

Shepherd, A., Ivins, E. R., Geruo, A., Barletta, V. R., Bentley, M. J., Bettadpur, S., Briggs, K. H., Bromwich, D. H., Forsberg, R., Galin, N., Horwath, M., Jacobs, S., Joughin, I., King, M. A., Lenaerts, J. T. M., Li, J., Ligtenberg, S. R. M., Luckman, A.,

Luthcke, S. B., McMillan, M., Meister, R., Milne, G., Mouginot, J., Muir, A., Nicolas, J. P., Paden, J., Payne, A. J., Pritchard, H., Rignot, E., Rott, H., Sandberg Sorensen, L., Scambos, T. A., Scheuchl, B., Schrama, J. O., Smith, B., Sundal, A. V., van Angelen, J. H., van de Berg, W. J., van den Broeke, M. R., Vaughan, D., Velicogna, I., Wahr, J., Whitehouse, P., Wingham, D. J., Yi, D., Y. D. & Zwally, H. 2012 A reconciled estimate of ice-sheet mass balance (science (1183)). *Science* **338** (6114), 1183–1189.

Smith, G. C., Roy, F., Mann, P., Dupont, F., Brasnett, B., Lemieux, J.-F., Laroche, S. & Bélair, S. 2014 A new atmospheric dataset for forcing ice–ocean models: Evaluation of reforecasts using the canadian global deterministic prediction system. *Quarterly Journal of the Royal Meteorological Society* **140** (680), 881–894.

Spielhagen, R. F., Werner, K., Srensen, S. A., Zamelczyk, K., Kandiano, E., Budeus, G., Husum, K., Marchitto, T. M. & Hald, M. 2011 Enhanced modern heat transfer to the arctic by warm atlantic water. *Science* **331** (6016), 450–453.

Straneo, F. 2006 Heat and freshwater transport through the central labrador sea. *Journal of Physical Oceanography* **36** (4), 606–628.

Straneo, F., Curry, R. G., Sutherland, D. A., Hamilton, G. S., Cenedese, C., Vge, K. & Stearns, L. A. 2011 Impact of fjord dynamics and glacial runoff on the circulation near helheim glacier. *Nature Geoscience* **4** (5), 322–327.

Straneo, F. & Heimbach, P. 2013 North atlantic warming and the retreat of greenland's outlet glaciers. *Nature* **504** (7478), 36–43.

Straneo, F., Sutherland, D. A., Holland, D., Gladish, C., Hamilton, G. S., Johnson, H. L., Rignot, E., Xu, Y. & Koppes, M. 2012 Characteristics of ocean waters reaching greenland's glaciers. *Annals of Glaciology* **53** (60), 202–210.

Sutherland, D. A., Straneo, F. & Pickart, R. S. 2014 Characteristics and dynamics of two major greenland glacial fjords. *Journal of Geophysical Research: Oceans* **119** (6), 3767–3791.

Swingedouw, D., Braconnot, P. & Marti, O. 2006 Sensitivity of the atlantic meridional overturning circulation to the melting from northern glaciers in climate change experiments. *Geophysical Research Letters* **33** (7), n/a–n/a, l07711.

Swingedouw, D., Rodehacke, C. B., Olsen, S. M., Menary, M., Gao, Y., Mikolajewicz, U. & Mignot, J. 2014 On the reduced sensitivity of the atlantic overturning to greenland ice sheet melting in projections: a multi-model assessment. *Climate Dynamics* Article in Press.

Van Den Broeke, M., Bamber, J., Ettema, J., Rignot, E., Schrama, E., Van Berg, W. J. D., Van Meijgaard, E., Velicogna, I. & Wouters, B. 2009 Partitioning recent greenland mass loss. *Science* **326** (5955), 984–986.

Weijer, W., Maltrud, M. E., Hecht, M. W., Dijkstra, H. A. & Kliphuis, M. A. 2012 Response of the atlantic ocean circulation to greenland ice sheet melting in a strongly-eddying ocean model. *Geophysical Research Letters* **39** (9).